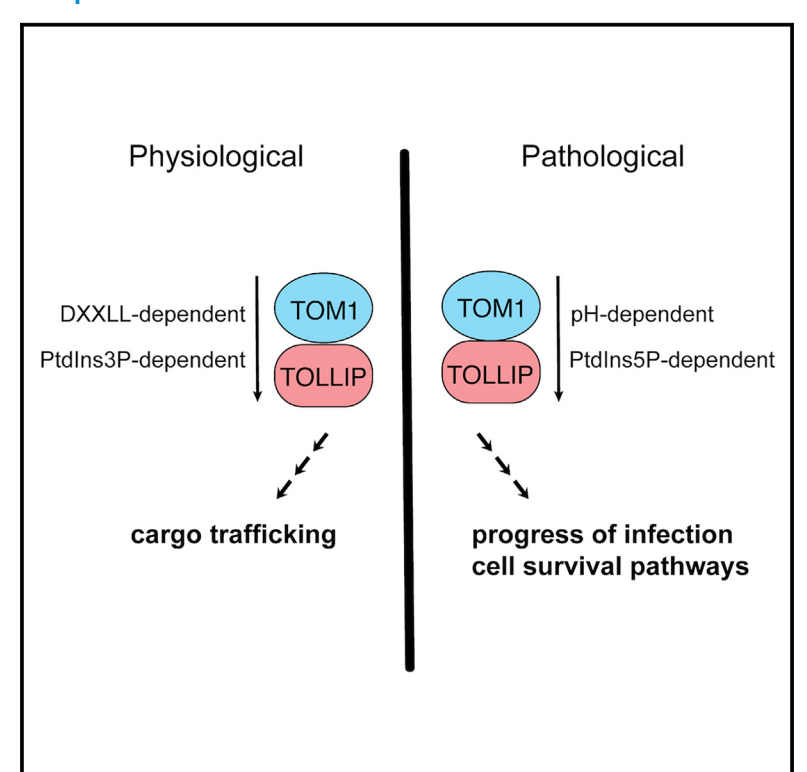
Structure

An internal linker and pH biosensing by phosphatidylinositol 5-phosphate regulate the function of the ESCRT-0 component TOM1

Graphical abstract



Authors

Wen Xiong, Tiffany G. Roach, Nicolas Ball, Marija Corluka, Josephine Beyer, Anne M. Brown, Daniel G.S. Capelluto

Correspondence

capellut@vt.edu

In brief

Xiong and Roach et al. report a DXXLL motif in TOM1 that increases its affinity for ubiquitin binding. They identify a PtdIns5P-binding site in TOM1 and demonstrate that its binding is maximal under acidic conditions. Furthermore, under these conditions, the TOM1-TOLLIP complex also interacts with the phosphoinositide.

Highlights

- Binding of TOM1 VHS to ubiquitin is enhanced by an internal DXXLL motif
- Binding of TOM1 to PtdIns5P is maximal under acidic conditions
- TOLLIP's binding to PtdIns5P also increases as pH acidifies
- A tight TOM1-TOLLIP complex binds to PtdIns5P under acidic conditions



Structure



Article

An internal linker and pH biosensing by phosphatidylinositol 5-phosphate regulate the function of the ESCRT-0 component TOM1

Wen Xiong,^{1,3,4} Tiffany G. Roach,^{1,4} Nicolas Ball,² Marija Corluka,¹ Josephine Beyer,¹ Anne M. Brown,² and Daniel G.S. Capelluto^{1,5,*}

¹Protein Signaling Domains Laboratory, Department of Biological Sciences, Fralin Life Sciences Institute, and Center for Soft Matter and Biological Physics, Virginia Tech, Blacksburg, VA 24061, USA

²Research and Informatics, University Libraries, Biochemistry Department, and Center for Drug Discovery, Virginia Tech, Blacksburg, VA 24061. USA

³Present address: Huffington Center on Aging, Baylor College of Medicine, Houston TX, 77030, USA

SUMMARY

Target of Myb1 (TOM1) facilitates the transport of endosomal ubiquitinated proteins destined for lysosomal degradation; however, the mechanisms regulating TOM1 during this process remain unknown. Here, we identified an adjacent DXXLL motif-containing region to the TOM1 VHS domain, which enhances its affinity for ubiquitin and can be modulated by phosphorylation. TOM1 is an endosomal phosphatidylinositol 5-phosphate (PtdIns5P) effector under *Shigella flexneri* infection. We pinpointed a consensus PtdIns5P-binding motif in the VHS domain. We show that PtdIns5P binding by TOM1 is pH-dependent, similarly observed in its binding partner TOLLIP. Under acidic conditions, TOM1 retained its complex formation with TOLLIP, but was unable to bind ubiquitin. *S. flexneri* infection inhibits pH-dependent endosomal maturation, leading to reduced protein degradation. We propose a model wherein pumping of H⁺ to the cytosolic side of endosomes contributes to the accumulation of TOM1, and possibly TOLLIP, at these sites, thereby promoting PtdIns5P- and pH-dependent signaling, facilitating bacterial survival.

INTRODUCTION

Cells employ various mechanisms to regulate the activity of integral membrane-bound proteins, including ion channels, G protein-coupled receptors, and receptor kinases, thereby modulating a wide array of intracellular signaling pathways. One of these regulatory mechanisms involves the covalent modification of membrane-bound receptors through a process known as ubiquitination. This modification marks the receptors as cargo. The attachment of ubiquitin molecules to these receptors serves as a recognition signal for adaptor proteins, which play a role in facilitating the sequestration and internalization of cargo through vesicular trafficking. Upon reaching the early endosomes, the cargo faces a crucial decision point. Cargo can either be directed toward the endosomal/lysosomal pathway for degradation or it may be returned to the plasma membrane for further engagement in intracellular signaling.¹

The degradation of cargo depends on the functionality of transient adaptor protein assemblies at the surface of early endosomes, collectively known as endosomal sorting complex required for transport (ESCRT). These ESCRT protein com-

plexes, namely ESCRT-0, -I, and -II, cooperatively transport cargo due to the presence of ubiquitin-binding domains within one or more proteins present in these assemblies. Furthermore, components of the ESCRT machinery, such as ESCRT-III and Vacuolar protein sorting 4 (Vps4), are responsible for budding deubiquitinated cargo-containing intralumenal vesicles into the lumen of the early endosomes, resulting in the formation of multivesicular bodies. These multivesicular bodies subsequently merge with late endosomes or lysosomes for cargo degradation. Through this process, ubiquitination and protein-lipid interactions play a pivotal role in coordinating the regulation of membrane trafficking and the degradation of proteins within lysosomes.²

The ESCRT-0 protein target of Myb1 (TOM1) is committed to facilitating the trafficking of endosomal cargo as evidenced by its role in transporting the delta opioid receptor, the auxin carrier protein, and interleukin-1 receptor to lysosomes; the latter receptor transportation requires TOM1 association with the Toll-interacting protein (TOLLIP).³ TOM1's ability to transport cargo is linked to its Vps27, HRS, and STAM (VHS) and GGA and TOM1 (GAT) domains, both of which possess ubiquitin-binding

⁴These authors contributed equally

⁵Lead contact

^{*}Correspondence: capellut@vt.edu https://doi.org/10.1016/j.str.2024.08.003





properties. In addition to cargo recognition, the GAT domain also mediates TOM1's interaction with TOLLIP. 4.5 This interaction inhibits the binding of TOLLIP to phosphatidylinositol 3-phosphate (PtdIns3P), a phospholipid that serves as a platform for recruiting TOLLIP at endosomal compartments. Interestingly, the TOM1 GAT domain cannot simultaneously bind both TOLLIP and ubiquitin, 4.6 suggesting that TOM1 can also participate in cargo trafficking independently of TOLLIP.

In addition to ubiquitin, the VHS domains of Golgi-localized, gamma-ear-containing, ADP-ribosylation-factor-binding (GGA) proteins recognize acidic-cluster dileucine (DXXLL) motifs located at the C-termini of transmembrane receptors, mediating their traffic between the *trans*-Golgi apparatus, and endosomes. However, VHS-containing proteins TOM1, hepatocyte growth factor-regulated tyrosine kinase substrate (HRS), and signal transducing adaptor molecule 1/2 (STAM1/2) do not bind to the C-terminal DXXLL motifs of transmembrane receptors. Furthermore, downstream of their hinge segments, GGAs also present an internal DXXLL motif that modulates transmembrane receptor-binding by interacting in *cis* with VHS domains.

Pathogens are known to manipulate host phosphoinositides to aid in their invasion, survival, evasion of the immune response, and replication. 10 During Shigella flexneri infection, the sorting function of TOM1 can be downregulated in a phosphatidylinositol 5-phosphate (PtdIns5P)-dependent manner. 11 S. flexneri invades host cells by internalizing within a vacuole. The bacterium disrupts and escapes from the vacuole by delivering the virulence factor IpgD, 12 a lipid phosphatase that increases endosomal PtdIns5P levels by ~200-fold, using host cellular phosphatidylinositol 4,5-bisphosphate. 13 The accumulation of PtdIns5P in endosomes leads to TOM1 and ligand-free epidermal growth factor receptor (EGFR) recruitment to these compartments. 11 Localization of TOM1 to endosomes depends on its VHS domain, which displays a preference for binding to PtdIns5P.11 The presence of TOM1 at endosomes inhibits host endosomal maturation and EGFR degradation, ultimately enhancing pathogen survival. 11 Intriguingly, a common PtdIns5P-dependent mechanism appears to be at play in other pathogen infections as well. 14 It remains unknown whether TOLLIP is hijacked during bacterial invasion, however, there is evidence to suggest that this could be the case. For instance, upon entry of Leishmania donovani into host cells, TOLLIP is impaired, leading to the inhibition of innate immunity and enabling parasite survival.¹⁸

Here, we used a combination of isothermal titration calorimetry (ITC), nuclear magnetic resonance (NMR) spectroscopy, and molecular dynamics (MD) simulations to investigate the function of a highly conserved DXXLL-containing VHS-GAT linker region in TOM1. We demonstrate that the DXXLL-containing region markedly enhanced ubiquitin binding to TOM1 VHS through the induction of local conformational changes. Using phosphomimetic mutations at the DXXLL region, we show that ubiquitin binding is downregulated by TOM1 phosphorylation. Moreover, we identified a PtdIns5P-binding motif in the TOM1 VHS domain and established that TOM1 binding to PtdIns5P is pH-dependent, with the strongest binding occurring under acidic conditions. The TOM1-binding partner, TOLLIP, was also found to interact with PtdIns5P in a pH-dependent manner. Thus, we propose that under normal physiological conditions,

TOM1 is recruited to endosomes through its interaction with Ptdlns3P-bound TOLLIP, facilitating cargo clustering at maturing endosomes. However, during bacterial infection, the increased levels of Ptdlns5P and the local acidic environment in the cytosol favor the sequestration of TOM1, and possibly TOLLIP, at the endosomal surface, thereby promoting bacterial survival.

RESULTS

A DXXLL motif-containing region enhances binding of VHS to ubiquitin

TOM1 functions as a ubiquitin-binding adaptor protein implicated in cargo transport on the surface of endosomes. It comprises a VHS domain followed by a central GAT domain, both of which can bind ubiquitin, and a long C-terminal domain (CTD) (Figure 1A). Our ITC experiments revealed that TOM1 binds ubiquitin exothermically with a dissociation constant (K_D) of \sim 40 μM and best fit with a stoichiometry of two binding sites with similar affinity for ubiquitin (Figure 1B; Table 1). Consistent with a previous report, 16 the isolated TOM1 VHS domain displayed weak binding to ubiquitin with a K_D of ${\sim}500~\mu\text{M}$, following a one-site binding model (Figure 1C; Table 1). Conversely, the TOM1 GAT domain bound ubiquitin with an estimated K_D of $\sim 100 \, \mu M$ (Figure 1D; Table 1), which falls within the range of affinity estimated for the GGA GAT domain interaction with ubiquitin, using the same methodology. 17 Hence, it appears that a region outside of the TOM1 VHS domain contributes to the overall tighter binding of the protein to ubiquitin. Binding to ubiquitin is independent of CTD, as its deletion did not affect the TOM1 binding affinity for ubiquitin (Table 1; Figure S1). An alignment of the sequence between the VHS and GAT domains revealed that the first 20 amino acids are highly conserved and contain a DXXLL motif, akin to those found in other sorting proteins (TOM1 DXXLL region, residues 150-169) (Figure S1). Notably, a TOM1 construct comprising the VHS domain followed by the DXXLL region (residues 11-169) increased the affinity for ubiquitin about 8-fold, with a K_D of \sim 70 μ M (Figure 1E; Table 1). To address the role of the DXXLL motif in this function, we introduced alanine mutations at residues D155, M158, and L159. Disruption of the DXXLL motif resulted in 4-fold reduction in the affinity of TOM1 VHS-DXXLL for ubiquitin (Figure 1F), closely mirroring that of TOM1 VHS for ubiquitin (Table 1). It is worth noting that the TOM1 DXXLL region alone did not bind to ubiquitin (Figure S1) nor affected the GAT domain binding properties (Figure S1) suggesting that it plays a structural function in enhancing the affinity of TOM1 VHS for ubiquitin.

To address the role of the DXXLL region for TOM1 VHS function in more detail, first, ¹⁵N-labeled ubiquitin was titrated with increasing concentrations of TOM1 VHS, without the DXXLL region, and two-dimensional heteronuclear single quantum coherence (HSQC) experiments were recorded. In the presence of TOM1 VHS, major chemical shift perturbations of ubiquitin resonances were observed for residues G47, K48, Q49, L50, E51, and L71 (Figures 2A and S2), which make up the ubiquitin-binding pocket (Figure 2B), in agreement with that observed for STAM VHS.¹⁸ Next, to elucidate the structural basis for how the DXXLL region enhances binding of the VHS domain to ubiquitin, HSQC experiments were performed by titrating ¹⁵N-ubiquitin with increasing concentrations of TOM1 VHS-DXXLL. Despite

Structure Article



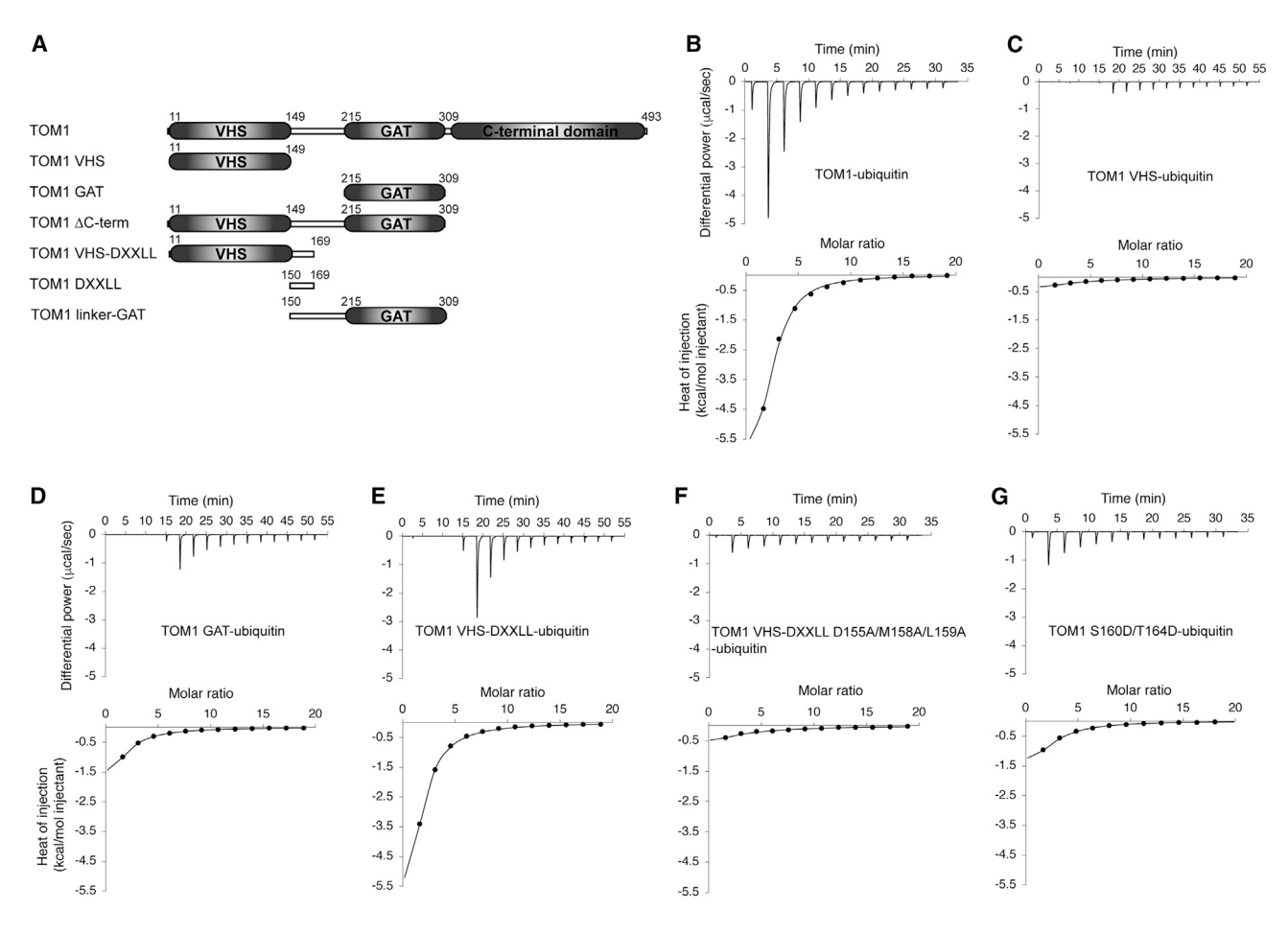


Figure 1. The TOM1 DXXLL region enhances VHS binding to ubiquitin

(A) Domain organization of TOM1 and derived constructs. Numbers indicate the amino acid boundaries of the TOM1 domains.

(B–G) ITC thermograms for TOM1 (B), TOM1 VHS (C), TOM1 GAT (D), TOM1 VHS-DXXLL (E), TOM1 VHS-DXXLL D155A/M158A/L159A (F), and TOM1 S160D/T164D (G) binding to ubiquitin. In all cases, top panel represents the ITC raw binding data for protein interactions, whereas the bottom is the integrated and

normalized data fit with a one set of sites binding model, with N fixed to either 1 or 2, depending upon the TOM1 construct tested. See also Figures S1-S3.

severe intensity loss of some of the ubiquitin resonances, the TOM1 VHS-DXXLL binding site was observed to be overlapping with the TOM1 VHS binding site (Figures 2C and S2). By calculating the intensity ratio of the resonance intensities of ubiquitin after addition of the TOM1 VHS-DXXLL over the resonance intensities of free ubiquitin, many ubiquitin resonances within the VHS binding pocket were observed to undergo intensity loss, specifically for a stretch of amino acids spanning residues L43 to E51 (red bar, Figure 2D), suggesting a stronger affinity interaction. By mapping these residues along with perturbed amino acid resonances, an extended binding pocket (Figure 2E) was observed. These results suggest that the presence of the DXXLL region increases the number of contacts of the VHS domain with ubiquitin.

To obtain structural input of the DXXLL region in TOM1 VHS, we recorded a near-UV circular dichroism (CD) spectra of TOM1 VHS and TOM1 VHS-DXXLL (residues 11–169). Data indicate that the DXXLL region induces changes in the TOM1 VHS spectrum spanning the aromatic band from 260 to 290 nm (Figure 3A). Although the DXXLL region contains one aromatic residue (F151; Figure S1), the observed spectral differences are

indicative of a DXXLL region-mediated conformational change in TOM1 VHS. This was subsequently confirmed by the evident shift of most of the TOM1 VHS-DXXLL resonances in HSQC spectra (Figure S3). To further interpret these structural changes, we investigated whether the DXXLL region alters the stability of the VHS domain through trypsin-limited proteolysis. Whereas the VHS domain displayed trypsin susceptibility at the lowest trypsin concentration tested, the presence of the DXXLL region provided more resistance to the enzyme (Figure 3B), suggesting that the DXXLL region increases the stability of the VHS domain.

The TOM1 structure was modeled at pH 7 using Robetta (Figures S4 and S5; Table S1, and Video S1), exhibiting 97.15% of favored Ramachandran plots with only 1.02% classified as outliers. Analysis of the MD simulations of TOM1 showed that the DXXLL region interacted with the VHS domain through 1000 ns (Figure 3C and Video S1). Immediately following postequilibration, T154 of the DXXLL motif formed a hydrogen bond with Q122 of the VHS domain, L159 formed a hydrogen bond with K79, T164 formed hydrogen bonds with both D38 and N80, and R167 formed a hydrogen bond with E42. (Figure 3C). At 300 ns, K79 established hydrogen bonds with D155



Table 1. Thermodynamic parameters for the binding of the indicated TOM1 constructs to ubiquitin

	N ^a	<i>K</i> _D (μM)	ΔH (kcal/mol)	ΔG (kcal/mol)	-TΔS (kcal/mol)
TOM1	2	44 ± 9	−7.7 ± 0.7	-6.0 ± 0.1	1.8 ± 0.6
TOM1 VHS	1	530 ± 109	-4.3 ± 1.3	-4.5 ± 0.1	-0.2 ± 1.4
TOM1 VHS-DXXLL	1	69 ± 9	-9.0 ± 2.9	-5.7 ± 0.1	3.3 ± 2.8
TOM1 VHS-DXXLL mutant ^b	1	296 ± 46	-3.4 ± 0.4	-4.8 ± 0.1	1.5 ± 0.5
TOM1 DXXLL	-	-	-	-	-
TOM1 GAT	1	101 ± 7	-3.3 ± 2.0	-5.5 ± 0.1	-2.2 ± 2.0
TOM1 linker-GAT	1	98 ± 20	-4.7 ± 1.1	-5.5 ± 0.1	-0.8 ± 1.2
ΤΟΜ1 ΔCTD	2	56 ± 4	-8.2 ± 0.8	-5.8 ± 0.1	2.4 ± 0.8
TOM1 S160D/T164D	2	106 ± 14	-2.8 ± 0.1	-5.4 ± 0.1	-2.6 ± 0.3

Values represent the mean of at least two independent experiments. Errors are displayed as standard deviation values.

and I162 that were maintained throughout the simulation. T154 remained in contact with Q122 in addition to new hydrogen bonds with S123 and D126, which were also maintained throughout the simulation. These two regions provide the main interactions which anchor the DXXLL region to the VHS domain. Collectively, these interactions provide further insight into the stability of the VHS and DXXLL regions and their contributions to ubiquitin binding mechanisms.

TOM1 is phosphorylated simultaneously at residues S160 and T164, downstream of the DXXLL motif (Figure S1), as identified during the cell cycle. 19 The phosphomimetic variant, TOM1 S160D/T164D, displayed a ~3-fold decrease in affinity for ubiguitin (Figure 1G; Table 1), suggesting that phosphorylation in the DXXLL region diminishes TOM1's function in cargo trafficking. The phosphomimetic variant of TOM1 displayed minor tertiary structural changes compared to its non-phosphorylated state (Figure 4A). In agreement with this observation and after equilibration at pH 7, the phosphorylated structure of TOM1 pS160/ pT164 showed minor structural changes of a magnitude comparable to those observed in the non-phosphorylated state. Notably, there was an increase in polar contacts between the linker region and the VHS domain when TOM1 was phosphorylated (Figure 4B). Both S160 and pS160 contacted K79 through their backbone oxygens, whereas pT164 engaged with residues M34, D38, and N80. Although contacts with D38 and N80 were present in non-phosphorylated structures after equilibration, they were transient throughout the simulation.

To gain further insights into the structural underpinning of the intramolecular contacts observed in TOM1 pS160/pT164, we also carried out HSQC titrations to identify the ubiquitin-binding residues within the TOM1 VHS domain. Most of the chemical shift changes in TOM1 VHS involved residues located primarily on and around α -helix 2, including W30, I32, N33, E35, D38, and I39 (Figures 4C and S6). To a lesser extent, resonance perturbations were also observed on α -helices 1, 4, and 5 such as those for G14 (α -helix 1), V73 and K79 (α -helix 4), and V89 (α -helix 5) (Figures 4C and S6). These results also align with structural studies of the STAM1 VHS domain, revealing the significance of W30, E35, and D38 in ubiquitin binding. MD simulations showed that residue D38 made contacts with pT164, whereas K79 interacted with both S160 and pS160 (Figure 4B). This sug-

gests that the presence of pS160 and pT164 within the ubiquitinbinding site in the VHS domain explains the observed reduction in affinity of TOM1 S160D/T164D for ubiquitin (Figure 1G).

As the cargo trafficking function of TOM1 may be influenced by phosphorylation within the DXXLL region, we asked whether this post-translational modification can also impact TOLLIP binding. Surface plasmon resonance (SPR) analysis indicated that the binding affinity of TOM1 S160D/T164D to TOLLIP was comparable to that measured for the TOM1-TOLLIP association (Figure S3; Table S2).

Identification of the PtdIns5P binding site in the TOM1 VHS domain

Whereas VHS domains exhibit a common right-handed superhelix consisting of eight helices, variations in ligand recognition arise from nonconserved amino acids located at α -helices 6 and 8²¹ or the absence of α -helix 8.²² The diverse array of VHS functions restricted to these regions is evident in NMR titrations of the ¹⁵N-labeled TOM1 VHS domain with soluble dibutanoyl PtdIns5P (Figures 5A and 5B). Leveraging nearly complete resonance assignments of the protein, 24 albeit weak, we have identified that the majority of TOM1 VHS residues perturbed by PtdIns5P reside within two distinct regions, α -helices 5–6 and α-helix 8. Among these, residues V89, E96, S97, V100, R101, L104, D143, G148, and L149 exhibited the largest resonance perturbations (Figures 5A-5C). Alternatively, some of these chemical shift perturbations may indicate local structural changes induced by PtdIns5P binding. Nonetheless, all NMR resonance perturbations appear to be confined to the second half of the VHS domain, distinct from the ubiquitin-binding site (Figures 4C and S6). Further analysis of the PtdIns5P-induced NMR chemical shift perturbations of the TOM1 VHS domain suggests the involvement of a region spanning residues 88-104 not only present in TOM1 orthologs TOM1-L1 and TOM1-L2, but also within the PtdIns5P-binding motif identified in 41 unrelated proteins (Figure 5D).²³

Binding of TOM1 to PtdIns5P is pH dependent

Consistent with our previous report,⁶ full-length TOM1 exhibited weak binding to soluble PtdIns5P (Figure S7). Furthermore, we carried out an analysis of TOM1 binding to PtdIns5P-containing liposomes with the liposome co-sedimentation assay. Under

^aN, stoichiometry of binding.

^bTOM1 VHS-DXXLL D155A/M158A/L159A.

Structure Article

CellPress

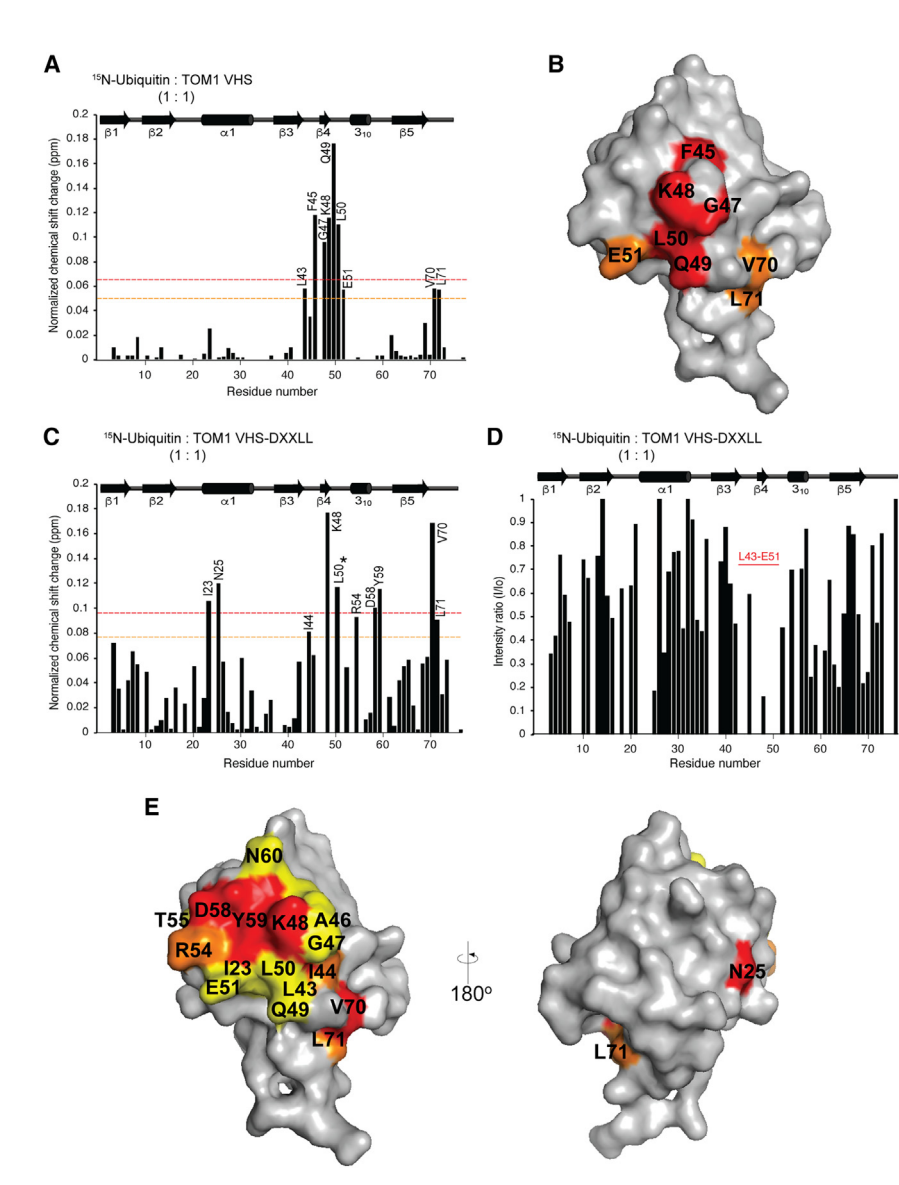


Figure 2. Contribution of the DXXLL region for the association of TOM1 VHS to ubiquitin (A) Normalized chemical-shift perturbations in the

(A) Normalized chemical-shift perturbations in the backbone amides of ubiquitin associated with TOM1 VHS binding. The orange and red dashed lines represent $\Delta\delta_{average}$ +1.0 × SD and $\Delta\delta_{average}$ +1.5 × SD, respectively.

(B) Surface structure of ubiquitin showing residues perturbed by TOM1 VHS with the color codes indicated in (A).

(C) Normalized chemical-shift perturbations in the backbone amides of ubiquitin associated with the TOM1 VHS-DXXLL. The colored dashed lines are defined in (A). *L50 could be identified by adjusting the phase value.

(D) Resonance intensity ratios for ubiquitin after the addition of TOM1 VHS-DXXLL. In (A), (C), and (D), secondary structure of ubiquitin is indicated on top.

(E) Two views of the surface structure of ubiquitin showing residues perturbed by the TOM1 VHS-DXXLL interaction. Residues with normalized chemical shift changes over $\Delta\delta_{average}+(1.5\times SD)$ and $\Delta\delta_{average}+(1\times SD)$ are colored with red and orange, respectively. Residues that underwent line broadening are highlighted in yellow. See also Figures S1–S3.

that the GAT domain contributes to the nonspecific lipid binding of TOM1, in line with previous observations. 11 Unfortunately, evaluation of the TOM1 GAT domain and TOM1 ΔVHS (residues 150–493) could not be performed as these proteins displayed very poor solubility at acidic pH.

To investigate whether the preference of TOM1 for binding to PtdIns5P at acidic pH conditions is due to a conformational change in the protein, we carried out near-UV CD structural analysis. However,

due to the limited solubility of TOM1 for CD analysis under acidic conditions, we performed structural analysis using the isolated VHS domain. Near-UV CD data revealed no discernible major structural changes as the protein transitioned from neutral to acidic conditions (Figure 6E). TOM1 is a monomer at neutral pH conditions (Figure S10). Gel filtration experiments revealed that the protein retains its monomeric state under acidic conditions (Figure S10). To confirm this observation, we performed 1000 ns MD simulations of monomeric TOM1 at pH5 and compared simulation results with those performed at a neutral pH (Video S1). The TOM1 VHS domain and linker region exhibited similar contacts under both pH conditions. However, while the linker and CTD remain in contact throughout the simulation time at pH 7, these regions did not interact at pH 5. In addition, the VHS and GAT domains remained in contact at pH 7, but they separated at approximately 350 ns. Within 400 ns MD simulation of TOM1 at pH 5, it was observed that the location of the PtdIns5P-binding region of the VHS domain, spanning residues 88-104, remains similarly positioned relevant to VHS compared to its location at neutral pH.

neutral pH conditions, TOM1 displayed poor binding to PtdIns5P, with most of the protein remaining in the supernatant. However, binding increased and gradually shifted to the pellet fraction as the pH of the buffer decreased, reaching close to 100% binding at pH 5 (Figures 6A and S8). A similar trend was observed for PtdIns5P-free liposomes, but to a much lesser extent (Figure 6A), suggesting that TOM1 exhibits increased nonspecific binding to lipid bilayers as the pH decreases. This behavior was not observed for the Vam7 PX domain, which binds to PtdIns3P,25 as the protein's binding to the lipid decreased upon reducing the pH of the buffer (Figures 6B, S7, and S9). To investigate whether the pH dependence of TOM1 binding to PtdIns5P is related to its VHS domain, we evaluated the binding of this region to the lipid. VHS domain binding to PtdIns5P showed pH dependence, mirroring the results obtained with TOM1 (Figures 6C and S8), but VHS lacked binding to PtdIns5P-free liposomes, indicating that other TOM1 regions bind other lipids nonspecifically. Removal of CTD (Figure 1A) mirrored the binding of TOM1 to PtdIns5P-containing and PtdIns5P-free liposomes (Figures 6D, S7, and S9), suggesting



Structure Article

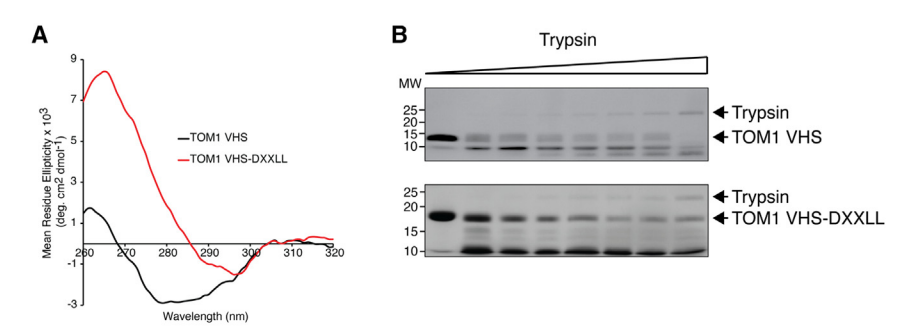
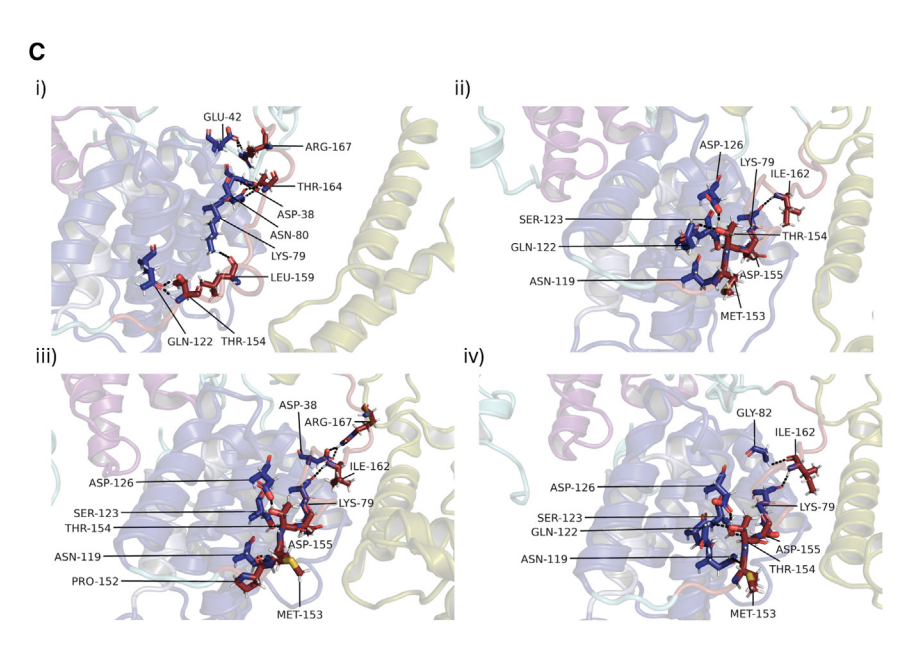


Figure 3. The TOM1 DXXLL region induces local conformational changes in the VHS domain

(A) Near-UV CD spectra of TOM1 VHS (black) and VHS-DXXLL (red).

(B) Analysis of trypsin-limited proteolysis of TOM1 VHS (top) and TOM1 VHS-DXXLL (bottom).

(C) Four snapshots of the MD simulation of TOM1 at 0 (i), 300 (ii), 600 (iii), and 1000 ns (iv). Contacts are denoted by black dashed lines. The DXXLL region is highlighted dark red, VHS in dark blue, and CTD in yellow. See also Figures S4–S6 and Table S1.



the host ubiquitin system to their advantage. Interestingly, TOM1 did not interact with ubiquitin under acidic conditions (Figures 7A and S13), suggesting that TOM1 is committed to PtdIns5P-dependent membrane binding.

The protein-protein docking analysis of ubiquitin to the TOM1 VHS-linker-GAT region revealed differences in docking behavior between pH 7 and 5 (Figure S14). Ubiquitin exhibited more favorable docking at pH 7 compared to pH 5, with tightly clustered poses observed in two replicate simulations at pH 7, whereas poor clustering was observed for all pH 5 structures, in agreement with the lack of interaction noted using ITC (Figure 7A). The interaction fingerprinting analysis of these docked poses showed good agreement between replicate 1 and 2 of TOM1 struc-

tures at pH 7. Ubiquitin displayed a preference for docking in specific regions of the VHS domain, such as residues 34–47, 78–85, and 125–132 (Figure S15), in close agreement with our NMR data (Figure 4C). In addition, ubiquitin interacted with TOM1 residues 159–172 (linker) and 298–306 (GAT) (Figure S15). In replicate 1, common independent interactions were observed with residues 180–184 and 238–245, while in replicate 2 independent interactions were found with residues 191–196. However, replicate 3 showed fewer interactions in these regions, with a higher frequency of outliers. In pH 5 replicate simulations for TOM1 interaction with ubiquitin, an infrequent but consistent interaction region spanning residues 230–270 of TOM1 was identified (Figure S15).

TOLLIP is also recognized as a cargo transporter, displaying a very strong affinity for TOM1⁶ (Table S2). To investigate whether TOLLIP maintains its binding capability with TOM1 under acidic conditions, we intended to carry out ITC and SPR analysis. However, due to the limited solubility of TOLLIP at pH 5, these methods were not feasible. Instead, we employed gel filtration analysis to evaluate the formation of the protein complex. Our data revealed that TOLLIP retained its dimeric state at pH 5²⁷ (Figure S16). Furthermore, we observed that TOM1 interacts with TOLLIP under both neutral and acidic conditions, resulting in the formation of a complex in both cases (Figure 7B) and that the TOM1 VHS domain was dispensable for interaction

To pinpoint the critical TOM1 VHS PtdIns5P-interacting residues within the PtdIns5P-binding motif, as identified by NMR. we screened an array of mutants using PtdIns5P-containing liposomes under acidic conditions. Of note, confirmation of the PtdIns5P-binding pocket in TOM1 VHS through HSQC titrations could not be carried out at pH 5 due to the insolubility of the free lipid under acidic conditions. Mutation at R101 significantly reduced PtdIns5P binding, and additional mutation at S97 further decreased binding (Figures 6F, S11, and S12). Mutations at L104, at the edge of PtdIns5P-binding motif, and at R146 and K147, both situated around α-helix 8, did not impact PtdIns5P binding (Figures 6F, S11, and S12). Structural analysis of the R101D and S97A/R101D PtdIns5P-binding mutants indicated that mutations did not alter the secondary structure of TOM1 VHS; hence, their functionality alone was targeted (Figure S11). Collectively, the PtdIns5P binding site on TOM1 VHS is situated at the boundaries of α-helices 5 and 6, with residue R101 likely engaging with the phosphoinositide head group through electrostatic contacts.

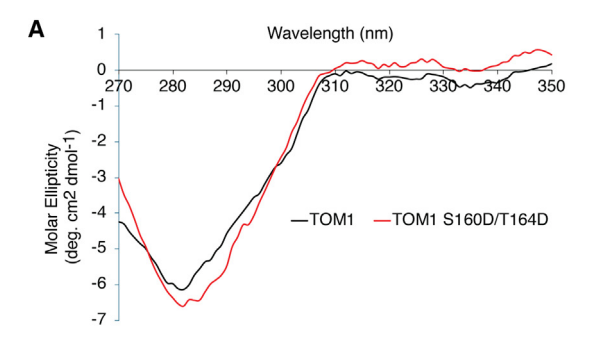
Under acidic conditions, TOM1 maintains its binding to TOLLIP, whereas its binding to ubiquitin is abolished

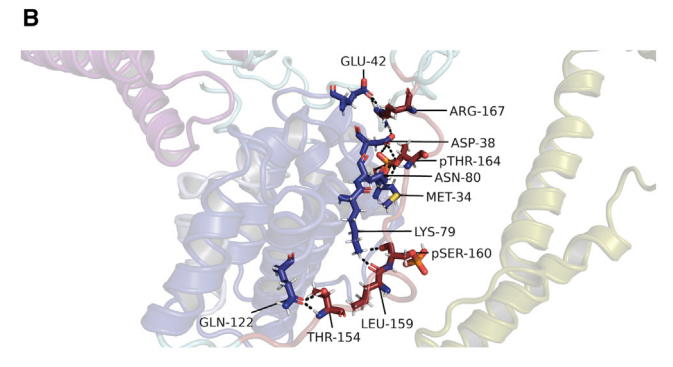
The ubiquitin machinery plays a crucial role in the host cellular defense program against bacterial infection. *Shigella* has evolved ubiquitin ligase-like enzymes that selectively exploit

Structure

Article







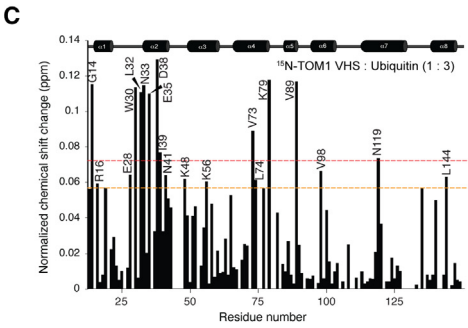


Figure 4. Structural impact of phosphorylation of the DXXLL region in TOM1

(A) Near-UV CD spectra of TOM1 (black) and TOM1 S160D/T164D (red). (B) Zoom-in view of the phosphorylated TOM1 VHS-linker region contacts at pH 7. The equilibrated structure of phosphorylated TOM1 is shown. Contacts are highlighted by black dashed lines, with VHS represented in dark blue, the

linker region in salmon, and CTD in yellow. (C) Histogram representing the normalized chemical-shift perturbations in the backbone amides of TOM1 VHS at 3-fold excess of ubiquitin. The orange and red dashed lines represent $\Delta\delta_{average} + (1.0 \times SD)$ and $\Delta\delta_{average} + (1.5 \times SD)$, respectively. Secondary structure of TOM1 VHS is indicated on top. See also Figure S3 and Table S2.

with TOLLIP at acidic conditions (Figure S16). Altogether, our findings suggest that even when TOM1 forms a complex with TOLLIP under acidic conditions, the VHS domain remains involved in binding to PtdIns5P.

TOLLIP exhibits broad preference for binding to phosphoinositides. ²⁸ Therefore, we evaluated the pH-dependent PtdIns5P-binding properties of TOLLIP. TOLLIP bound PtdIns5P at physiological pH (Figures 7C and S17), consistent with previous findings. ²⁸ Interestingly, binding of TOLLIP to the phosphoinositide was significantly enhanced under acidic conditions, similar

to that observed with TOM1 (Figure 6A), albeit the enhancement displayed was gradual (Figures 7C and S17).

Next, we asked whether the TOM1-TOLLIP complex could also associate to PtdIns5P under acidic conditions. To address this, we cross-linked these proteins at a 1:1 molar ratio, incubated them in the absence or presence of PtdIns5P liposomes at acidic conditions, and visualized the resulting centrifuged fractions using SDS-PAGE. The crosslinked TOM1-TOLLIP complex showed significant binding to PtdIns5P liposomes under these conditions (Figures 7D and S17). Considering the contribution of the TOM1 GAT domain to nonspecific binding (Figure 6A), these findings support the observation that the TOM1 GAT domain is committed to binding to the TOLLIP C2 and TBD regions.⁶ Taken all together, we propose a model in which, under physiological conditions (Figure 8A), TOM1 is recruited by PtdIns3P-bound TOLLIP at endosomal compartments, favoring cargo clustering at maturing endosomes. The DXXLL region, downstream of the VHS domain, enhances ubiquitin interactions, which in turn, are modulated by phosphorylation of the DXXLL region. Under bacterial infection conditions, however, PtdIns5P accumulates at endosomes (Figure 8B). We propose that PtdIns5P accumulation stimulates Na+/H+ exchanger (NHE) activation, increasing lumenal pH with a concomitant reduction of endosomal maturation. Accumulation of PtdIns5P and local acidic environment favor TOM1 and, possibly TOLLIP, sequestration, which promote ligand-independent EGFR receptor-mediated signaling and cell survival.

DISCUSSION

TOM1 recognizes cargo through its ubiquitin-binding VHS and GAT domains. We identified a highly conserved region downstream of the VHS domain containing a canonical DXXLL motif, known for its role in protein sorting in unrelated proteins. This motif specifically enhanced the affinity of the TOM1 VHS domain for ubiquitin to levels comparable to the GAT domain. TOM1 displayed even higher ubiquitin binding affinity, in line with what was observed in GGA3, where its VHS and GAT domains cooperatively bind to ubiquitin, but unlike TOM1, the individual VHS and GAT domains of GGA3 show limited or no ubiquitin binding. ²⁹

The length of the linker region in tandem with ubiquitin interacting motifs of proteins plays a crucial role in their ability to bind ubiquitin chains. 30,31 Interestingly, the linker sequence between the GGA3 VHS and GAT domains consists of 24 amino acids, whereas the TOM1 VHS-GAT linker spans 66 amino acids. Unlike TOM1, the GGA3 linker region contains 9 proline residues out of 24, suggesting a likely disordered nature. Thus, this region in TOM1 may facilitate cooperativity between the VHS and GAT domains, allowing for greater flexibility to accommodate ubiquitin binding. Our MD simulations of TOM1 revealed dynamic behavior in the DXXLL, GAT, and CTD regions, with VHS displaying comparatively much lower mobility (Figure S4; Video S1). The longer linker sequence in TOM1 suggests that its VHS and GAT domains could bind ubiguitin moieties independently. The decoupling of the TOM1 VHS and GAT domains may be favored by the outward orientation of the α -helix 8 in the VHS domain, influencing the conformation of the interdomain linker.



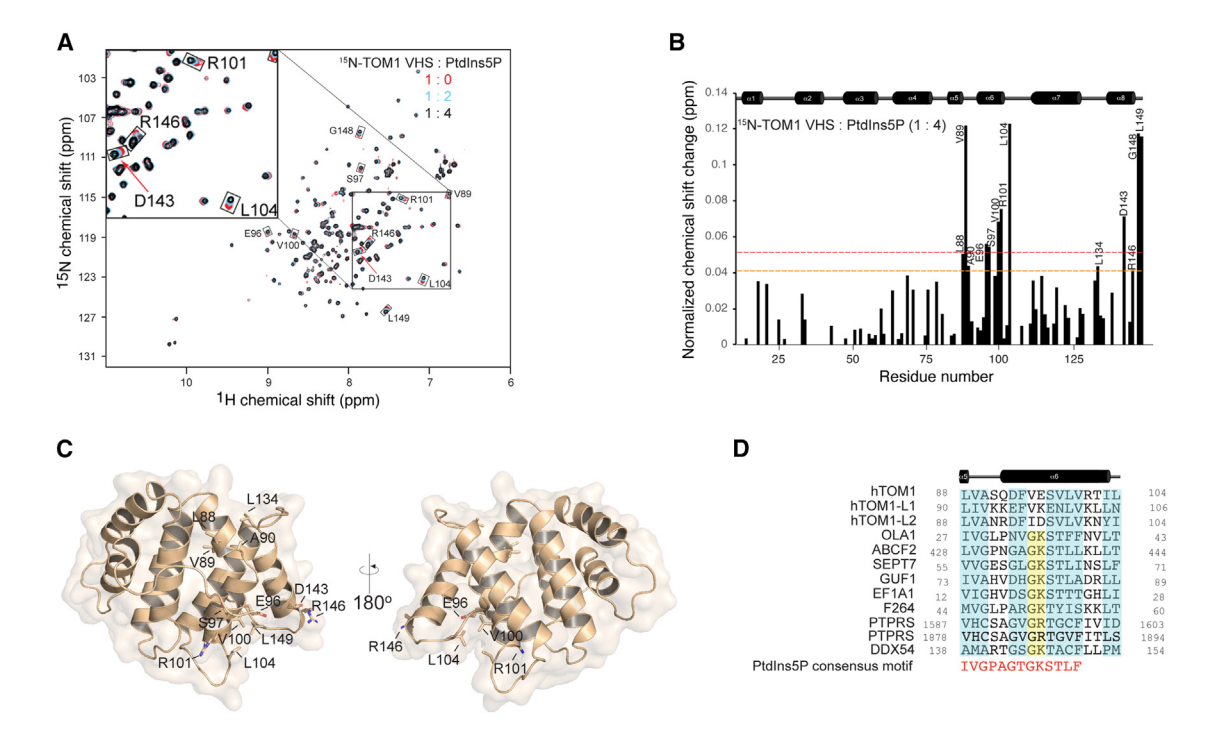


Figure 5. Identification of the PtdIns5P-binding site in the TOM1 VHS domain

(A) Overlay of HSQC spectra of the ¹H-¹⁵N TOM1 VHS domain in the absence (red) and presence of 2- (cyan) and 4-fold (black) of water-soluble PtdIns5P. Inset: Close-up view of the chemical shift changes for V89, R101, L104, D143, and R146.

(B) Histogram representing the normalized chemical-shift perturbations in the backbone amides of TOM1 VHS at 4-fold excess of PtdIns5P. The orange and red dashed lines represent $\Delta \delta_{average} + (1.0 \times SD)$ and $\Delta \delta_{average} + (1.5 \times SD)$, respectively. Secondary structure of TOM1 VHS is indicated on top.

(C) Two views of the cartoon/surface structure of the TOM1 VHS domain showing residues perturbed by PtdIns5P.

(D) Sequence alignment of proteins containing PtdIns5P consensus motifs. Residues conserved across sequences are shaded in light blue. The conserved GK sequence is highlighted in yellow. The consensus PtdIns5P sequence reported by Herianto et al.²³ is shown in red. OLA1, obg-like ATPase 1; ABCF2, ATP-binding cassette sub-family F member 2; SEPT7, septin 7; GUF1, GTP-binding elongation factor 1; EF1A1, elongation factor 1 alpha 1; F264, 6-phosphofructo-2-kinase/fructose-2,6-bisphosphatase 4; PTPRS, receptor-type tyrosine-protein phosphatase S; DDX54, ATP-dependent RNA helicase DDX54. The secondary structure of TOM1 is shown on top of the alignment. See also Figures S7 and S11.

Our data show that the ubiquitin binding site in TOM1 VHS maps in and around $\alpha\text{-helices 2}$ and 4 (Figure 4C), representing a conserved feature of VHS domains. Similarly, the TOM1 VHS domain binding site in ubiquitin, located on and around $\beta\text{-strand 4}$ (Figures 2A and 2B), is a conserved feature. The DXXLL region markedly enhances the affinity of the VHS domain for ubiquitin, likely through additional interactions involving $\alpha\text{-helix 1, 3}_{10}$, and the flexible C-terminal region of ubiquitin (Figure 2C).

The VHS domain of the GGA protein family has been reported to interact with DXXLL motifs present in membrane receptors. ^{32–34} This interaction is proposed to occur by the motif protruding into the groove of the VHS domain, formed between α-helices 6 and 8, through hydrophobic interactions with residues located at the base of this binding pocket. ^{32–34} In the case of TOM1, such interactions may promote VHS-ubiquitin interactions for cargo sorting when the GAT domain is not available for this purpose. TOM1 binds TOLLIP through its GAT domain, which in turn associates with the TOLLIP TBD and C2 domains. ⁶ Consequently, when TOM1 is in a TOLLIP-bound state, the TOM1 GAT domain is unlikely to bind ubiquitin moieties. This underscores the critical role of the DXXLL region in cargo transport by TOM1, particularly when in complex with

TOLLIP. The function of the DXXLL region of TOM1 may be regulated by phosphorylation at S160 and T164, ¹⁹ further evidenced by the weakened ubiquitin interaction observed when phosphomimetics were used (Figure 1G). Phosphorylation of TOM1 did not alter TOLLIP binding, which reinforces our findings indicating that the GAT domain, which is necessary and sufficient for TOLLIP binding, ⁶ is not regulated for ubiquitin binding by the DXXLL region. However, it remains plausible that phosphorylation of TOM1 in the DXXLL region could lead to post-translational modifications or subcellular relocalization of TOLLIP to other protein complexes. ³⁵

Early studies on the TOM1 VHS domain revealed a positively charged patch on one side, encompassing α -helices 3, 4, 6, and 7, and a negatively charged region, around α -helix 2, on the opposite side. ³⁶ Although α -helix 8 points away from the structure, the space between α -helix 8 and α -helices 6 and 7 is enriched with hydrophobic residues. In our present study, NMR experiments identified a PtdIns5P binding groove primarily formed by TOM1 VHS residues located on α -helix 6. Comparison between the PtdIns5P-binding region of TOM1 VHS and the proposed PtdIns5P-interacting consensus motif²³ reveals that TOM1 VHS displays a canonical PtdIns5P-binding region, lacking the consensus GK sequence found in the Walker A motif

Structure Article



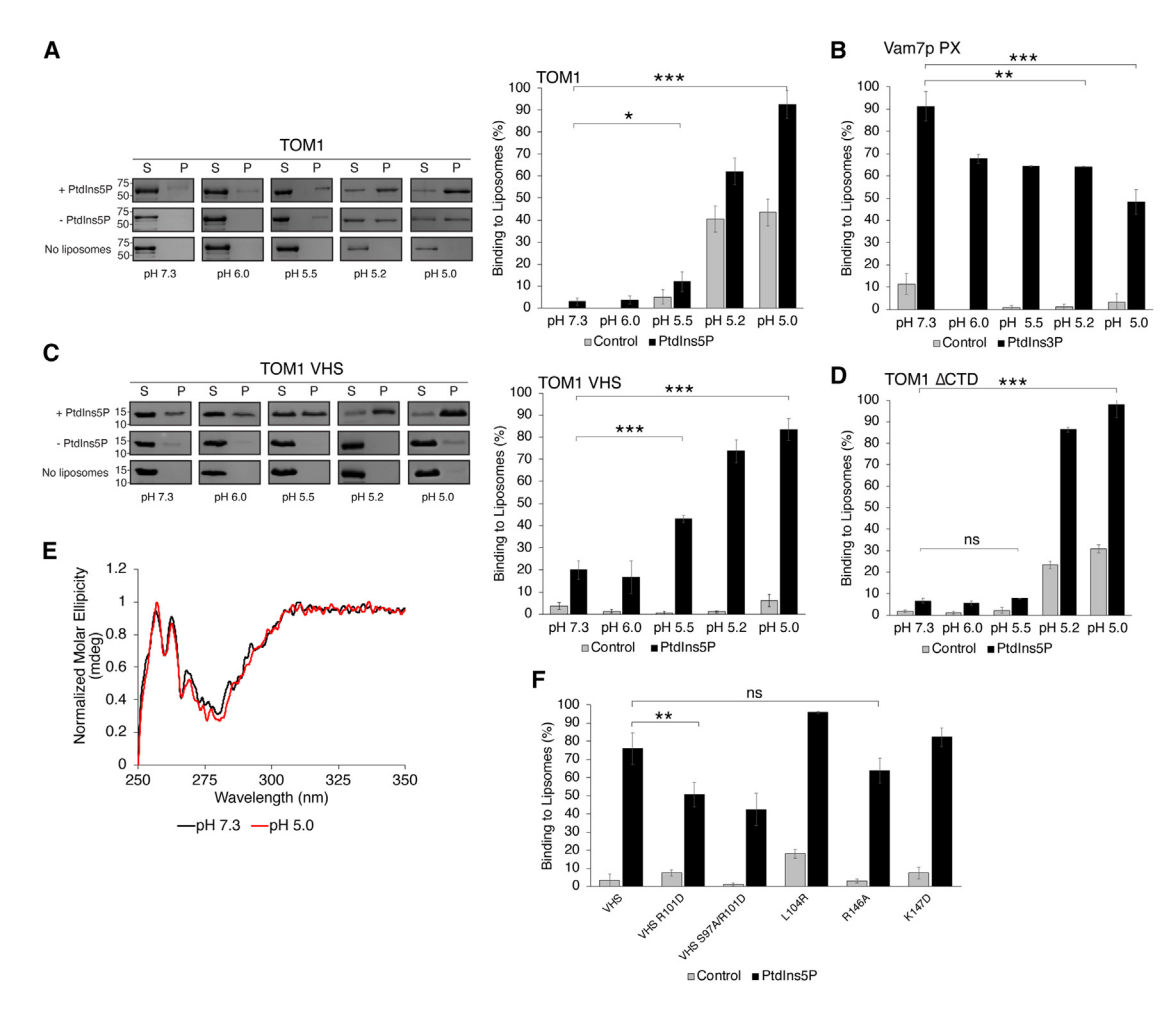


Figure 6. Binding of TOM1 to PtdIns5P is pH dependent

(A) Left, Analysis of the liposome co-sedimentation assay for TOM1 with PtdIns5P-containing and PtdIns5P-free liposomes or TOM1 alone. S, supernatant; P, pellet. Right, quantification of the intensity of the TOM1 bands obtained by densitometry.

- (B) Quantification of the intensity of the Vam7p PX domain bands under the indicated experimental conditions.
- (C) Left, Analysis of the liposome co-sedimentation assay for the TOM1 VHS domain with PtdIns5P-containing and PtdIns5P-free liposomes or TOM1 VHS alone. S, supernatant: P, pellet. Right, quantification of the intensity of the TOM1 VHS bands obtained by densitometry.
- (D) Quantification of the intensity of the TOM1 Δ CTD bands under the indicated experimental conditions. In all cases, data represent the mean of at least three independent experiments.
- (E) Overlay of near-UV CD spectra of TOM1 VHS at pHs 7.3 (black) and 5.0 (red).
- (F) Quantification of the intensity of the TOM1 VHS domain and mutants for PtdIns5P binding at pH 5.0. When indicated, error bars represent the standard deviation from at least three independent experiments. *p < 0.05; **p < 0.01; ***p < 0.001; ns, not significant. See also Figures S7–S12.

and, based on our NMR data, likely extended by an additional four residues (Figure 5D). Nevertheless, the identified Ptdlns5P-binding motif in TOM1 remains conserved among members of the TOM1 family proteins, such as TOM1-L1 and TOM1-L2 (Figure 5D). Also, this motif shares common residues with other VHS-containing proteins, including GGA1 and GGA3, which bear the consensus GK sequence. Taken together, data suggest that, in addition to TOM1, other VHS-containing proteins could recognize phosphoinositides under conditions such as local acidification states.

Boal et al. reported that the TOM1 VHS domain binds phosphoinositides, exhibiting strong preference for PtdIns5P, whereas the GAT domain binds nonspecifically to monophosphorylated phosphatidylinositols.¹¹ However, no data are

available for the full-length protein. Our liposome co-sedimentation assays revealed that TOM1 significantly binds PtdIns5P under acidic conditions. The major contributor for this association is the VHS domain, whereas the GAT domain displays nonspecific binding to lipid bilayers, consistent with previous findings. ¹¹ Upon host invasion, *S. flexneri* secretes IpgD, resulting in the endosomal accumulation of PtdIns5P. By an unknown mechanism, accumulation of PtdIns5P blocks endosomal maturation, impairing the lysosomal degradative pathway. ¹¹ Endosomal maturation relies on the capacity of endosomes to acidify their lumenal pH, primarily mediated by the V-type H⁺-ATPase pumps, with NHEs contributing by expelling protons while allowing Na⁺ ions to enter the endosomal lumen. ³⁸ Inhibition of endosome maturation involves the



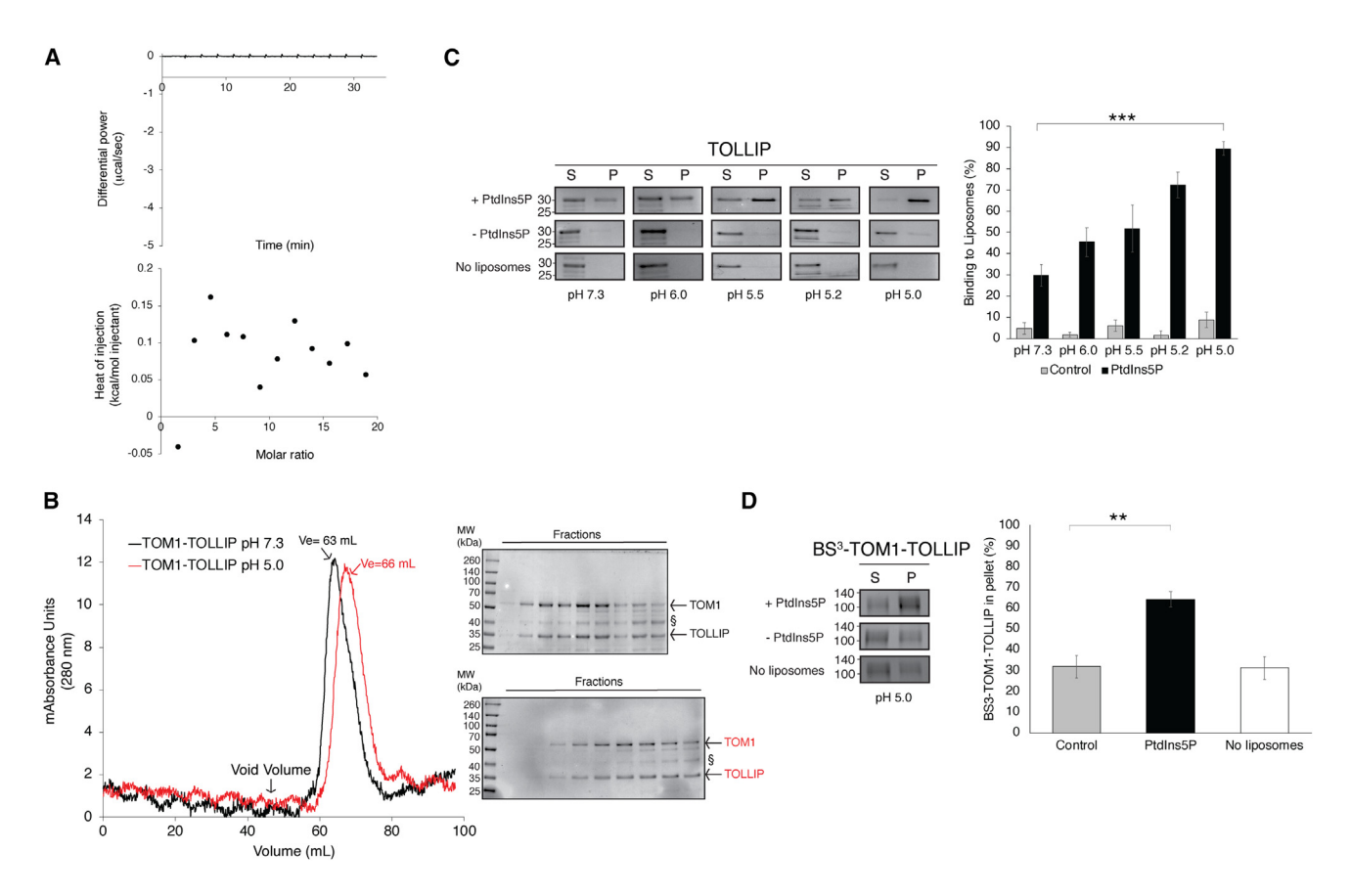


Figure 7. Additional features of TOM1 and TOLLIP at acidic conditions

(A) ITC analysis for the interaction of TOM1 with ubiquitin at acidic conditions.

(B) Left, Analysis of the liposome co-sedimentation assay for TOLLIP with PtdIns5P-containing and PtdIns5P-free liposomes or TOLLIP alone. S, supernatant; P, pellet. Right, quantification of the intensity of the TOLLIP bands obtained by densitometry.

(C) Size-exclusion chromatogram showing the elution profile of the TOM1-TOLLIP complex at pHs 7.3 (black) and 5.0 (red). Ve, elution volume. Right, Analysis of the fractions of each peak at pHs 7.3 (top) and 5.0 (bottom).

(D) Binding of the TOM1-TOLLIP crosslinked complex to PtdIns5P at pH 5.0 evaluated through the liposome co-sedimentation assay. In all cases, data represent the results of three independent experiments and error bars, when indicated, represent their standard deviation. **p < 0.01; ***p < 0.001. See also Figures S13–S17.

activation of NHEs.³⁹ The regulatory function of NHEs in maintaining intracellular pH is dependent on phosphoinositides.^{40,41} Interestingly, the activity of Nhx1, a yeast endosomal NHE, is essential for the targeting of the phosphoinositide-binding cargo trafficking protein Vps27p to the endosomal surface.⁴² Similarly, the mammalian cargo trafficking protein HRS is preferentially targeted to the endosomal membrane surface under local acidic conditions,⁴³ aligning with our proposed model (Figure 8B). Delivery of TOM1 to PtdIns5P-enriched endosomes blocks EGFR degradation as well as fluid-phase endocytosis.¹¹ Thus, it is plausible that TOM1 is recruited to a PtdIns5P- and NHE-enriched region of the cytosolic leaflet of endosomes, where it facilitates ligand-independent EGFR signaling from these organelles used by *S.flexneri* for host cell survival.

By mutating residues located on α -helix 3 (K48, R52, K58, and K59), Boal et al. observed a reduction in the binding of the VHS domain to PtdIns5P, and to a lesser degree, to other phosphatidylinositol monophosphates. ¹¹ However, it is reasonable to argue that mutagenesis of these residues may disrupt the sec-

ondary structure of the VHS domain, potentially leading to a loss of lipid binding due to structural perturbations. Instead, we targeted residues in the VHS domain whose NMR resonances were severely perturbed by the addition of Ptdlns5P. Mutations at S97 and R101 within $\alpha\text{-helix}$ 6, significantly affected lipid binding without altering the structure of the VHS domain under acidic conditions, supporting the identification of the Ptdlns5P-interacting motif in the TOM1 VHS domain.

The EEA1 FYVE and the FAPP1 PH domains bind phosphoinositides in a pH-dependent manner, with the strongest interaction occurring under low pH conditions. We histor is driven by histidine residues, which undergo protonation under acidic conditions. We explored this possibility by replacing H65 and H114, within the TOM1 VHS domain, with alanine, and performed the liposome co-sedimentation assay at pH 5. Binding to PtdIns5P remained unchanged compared to that observed for the TOM1 VHS domain (data not shown). Recent studies suggest that phosphatidylinositol monophosphates are particularly sensitive to pH. 46 Changes in pH, along with lipid composition in membranes, severely affect the

Structure Article



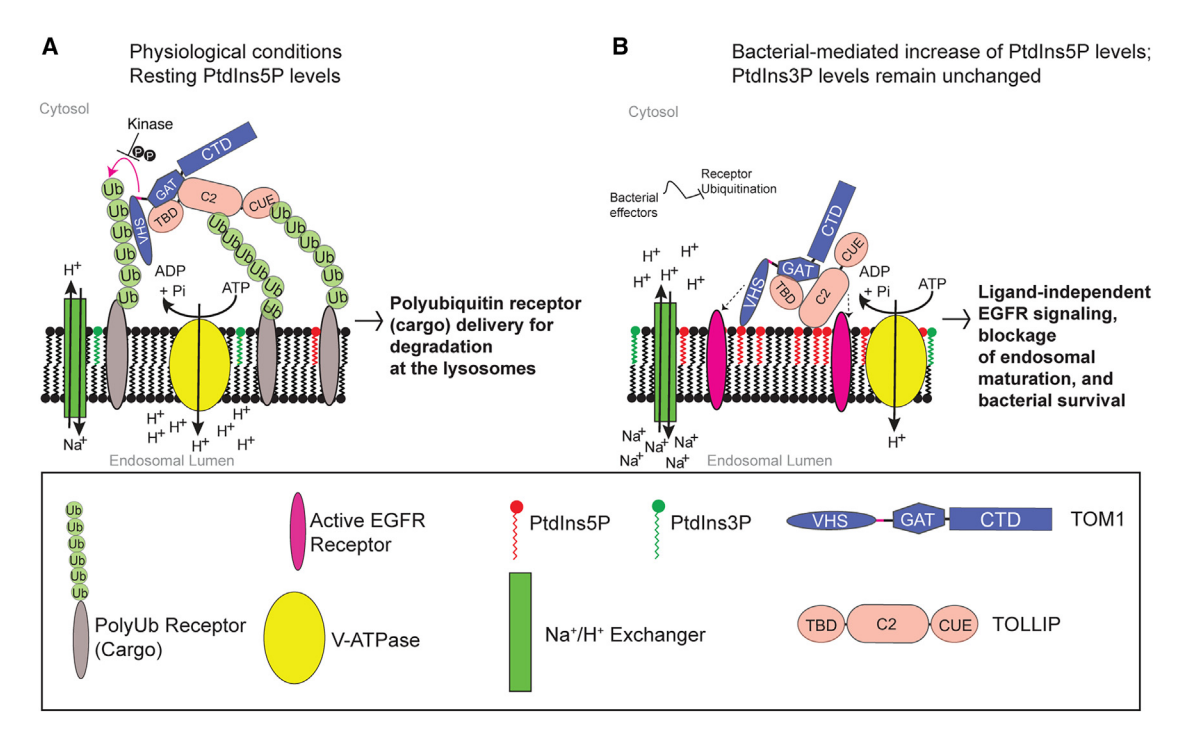


Figure 8. pH governs the cargo trafficking function of TOM1 and TOLLIP

(A and B) Model for pH-dependent regulation of endosomal cargo trafficking. Left, cargo is transported to early endosomes through vesicular transport. TOM1 is recruited by PtdIns3P-bound TOLLIP in these compartments, facilitating cargo clustering at maturing endosomes. The DXXLL region, downstream of the VHS domain, enhances ubiquitin interactions. Phosphorylation at the indicated sites downregulates TOM1-mediated cargo trafficking. Right, under bacterial infection conditions, PtdIns5P accumulates at early endosomes. Endosomal maturation is impaired by the activity of the phosphoinositide-dependent NHE pump. Ubiquitination processes are subverted by bacterial effectors. PtdIns5P accumulation favors TOM1 and TOLLIP sequestration, promoting ligand-independent receptor-mediated signaling and cell survival.

ionization properties of phosphatidylinositol monophosphates. For example, phosphatidylethanolamine reduces the pKa2 values of the phosphatidylinositol monophosphates. ⁴⁶ Therefore, it is possible that, under acidic conditions, the binding of TOM1 to PtdIns5P might depend on both pH-dependent conformational changes of the protein, as observed in CD spectra (Figure 6D), and the membrane lipid composition.

Under acidic conditions, we showed that TOM1 was unable to bind ubiquitin. Unfortunately, we were unable to test this function in TOLLIP, as the protein exhibited limited solubility for the concentration required for ITC analysis. Nevertheless, the TOM1 result aligns with the observed delay in endosomal maturation and reduced ubiquitin-dependent protein turnover under S. flexneri infection. 11 Furthermore, we found that, under acidic conditions, TOLLIP also displayed preferential binding to PtdIns5P and bound to TOM1, which, as a complex, retained its ability to bind to the phosphoinositide. This suggests the possibility that TOLLIP is also sequestered at endosomal compartments during S. flexneri infection (Figure 8B). As highlighted by Hurley and colleagues, VHS domains likely serve as "low efficiency membrane-binding domains". 36 In the case of TOM1, this deficiency in membrane binding could be compensated by high-affinity partners such as TOLLIP.

STAR***METHODS**

Detailed methods are provided in the online version of this paper and include the following:

- KEY RESOURCES TABLE
- RESOURCE AVAILABILITY
 - Lead contact
 - Materials availability
 - Data and code availability
- EXPERIMENTAL MODEL AND STUDY PARTICIPANT DETAILS
- METHOD DETAILS
 - o Cloning and mutagenesis
 - o Protein expression and purification
 - Isothermal titration calorimetry
 - NMR spectroscopy
 - Circular dichroism
 - Limited trypsin proteolysis
 - Molecular dynamics simulations
 - Surface plasmon resonance
 - Liposome co-sedimentation assay
 - Chemical crosslinking
 - Analytical size-exclusion chromatography
 - Visualization
- QUANTIFICATION AND STATISTICAL ANALYSIS

SUPPLEMENTAL INFORMATION

Supplemental information can be found online at https://doi.org/10.1016/j.str. 2024.08.003.

ACKNOWLEDGMENTS

We thank Dr. Wei Song, Dr. Tuo-Xian Tang, Evan Littleton, and Bridget Spruill for their initial contribution to this work. Funding for this study was obtained through grant 2337495 from the National Science Foundation, the Virginia





Academy of Sciences, the Mary Louise Andrews Cancer Research Award, and the 4-VA Award to D.G.S.C. W.X. was supported by the Noel Krieg and the Graduate Student Doctoral Assistantship fellowships. T.G.R. was supported by the NIH Initiative for Maximizing Student Development, the Multicultural Academic Opportunities Program at Virginia Tech, and the George E. & Hester B. Aker fellowship. J.B. was supported by Fralin SURF and the Luther and Alice Hamlett research funding.

AUTHOR CONTRIBUTIONS

W.X., T.G.R., A.M.B., and D.G.S.C. conceived the experiments. W.X., T.G.R., M.C., and J.B. expressed and purified proteins. W.X. and T.G.R. performed and analyzed NMR, CD, and ITC experiments. J.B. performed trypsin limited proteolysis. T.G.R. performed and analyzed SPR experiments. T.G.R. and M.C. performed and analyzed analytical size-exclusion chromatography and liposome co-sedimentation assays. N.B. and A.M.B. performed, processed, and visualized molecular docking and MD simulations. D.G.S.C. wrote the manuscript with contributions from all co-authors. All authors concur that the contributions of W.X. and T.G.R. are equal, and that their positions on the author list can be swapped on curricula vitae, websites, reports, and other relevant platforms if desired.

DECLARATION OF INTERESTS

The authors declare no competing interests.

Received: May 15, 2024 Revised: July 11, 2024 Accepted: August 2, 2024 Published: August 28, 2024

REFERENCES

- 1. Berlin, I., Sapmaz, A., Stevenin, V., and Neefjes, J. (2023). Ubiquitin and its relatives as wizards of the endolysosomal system. J. Cell Sci. 136, jcs260101. https://doi.org/10.1242/jcs.260101.
- 2. De Craene, J.O., Bertazzi, D.L., Bar, S., and Friant, S. (2017). Phosphoinositides, major actors in membrane trafficking and lipid signaling pathways. Int. J. Mol. Sci. 18, 634. https://doi.org/10.3390/
- 3. Roach, T.G., Lång, H.K.M., Xiong, W., Ryhänen, S.J., and Capelluto, D.G.S. (2021). Protein Trafficking or cell signaling: A dilemma for the adaptor protein TOM1. Front. Cell Dev. Biol. 9, 643769. https://doi.org/ 10.3389/fcell.2021.643769.
- 4. Katoh, Y., Shiba, Y., Mitsuhashi, H., Yanagida, Y., Takatsu, H., and Nakayama, K. (2004). Tollip and Tom1 form a complex and recruit ubiquitin-conjugated proteins onto early endosomes. J. Biol. Chem. 279,
- 5. Yamakami, M., Yoshimori, T., and Yokosawa, H. (2003). Tom1, a VHS domain-containing protein, interacts with tollip, ubiquitin, and clathrin. J. Biol. Chem. 278, 52865-52872. https://doi.org/10.1074/jbc.
- 6. Xiao, S., Brannon, M.K., Zhao, X., Fread, K.I., Ellena, J.F., Bushweller, J.H., Finkielstein, C.V., Armstrong, G.S., and Capelluto, D.G.S. (2015). Tom1 modulates binding of Tollip to phosphatidylinositol 3-phosphate via a coupled folding and binding mechanism. Structure 23, 1910-1920. https://doi.org/10.1016/j.str.2015.07.017.
- 7. Guo, Y., Sirkis, D.W., and Schekman, R. (2014). Protein sorting at the trans-Golgi network. Annu. Rev. Cell Dev. Biol. 30, 169-206. https://doi. org/10.1146/annurev-cellbio-100913-013012.
- 8. Bonifacino, J.S. (2004). The GGA proteins: adaptors on the move. Nat. Rev. Mol. Cell Biol. 5, 23-32. https://doi.org/10.1038/nrm1279.
- 9. Doray, B., Bruns, K., Ghosh, P., and Kornfeld, S.A. (2002). Autoinhibition of the ligand-binding site of GGA1/3 VHS domains by an internal acidic cluster-dileucine motif. Proc. Natl. Acad. Sci. USA 99, 8072-8077. https://doi. org/10.1073/pnas.082235699.

- 10. Qiu, S., and Côté, M. (2019). From hitchhiker to hijacker: pathogen exploitation of endosomal phosphoinositides. Biochem. Cell Biol. 97, 1-9. https://doi.org/10.1139/bcb-2017-0317.
- 11. Boal, F., Mansour, R., Gayral, M., Saland, E., Chicanne, G., Xuereb, J.M., Marcellin, M., Burlet-Schiltz, O., Sansonetti, P.J., Payrastre, B., and Tronchère, H. (2015). TOM1 is a PI5P effector involved in the regulation of endosomal maturation. J. Cell Sci. 128, 815-827. https://doi.org/10. 1242/jcs.166314.
- 12. Ashida, H., Mimuro, H., and Sasakawa, C. (2015). Shigella manipulates host immune responses by delivering effector proteins with specific roles. Front. Immunol. 6, 219. https://doi.org/10.3389/fimmu.2015.00219.
- 13. Ramel, D., Lagarrigue, F., Pons, V., Mounier, J., Dupuis-Coronas, S., Chicanne, G., Sansonetti, P.J., Gaits-lacovoni, F., Tronchère, H., and Payrastre, B. (2011). Shigella flexneri infection generates the lipid PI5P to alter endocytosis and prevent termination of EGFR signaling. Sci. Signal. 4, ra61. https://doi.org/10.1126/scisignal.2001619.
- 14. Hasegawa, J., Strunk, B.S., and Weisman, L.S. (2017). PI5P and PI(3,5)P2: Minor, but essential phosphoinositides. Cell Struct. Funct. 42, 49-60. https://doi.org/10.1247/csf.17003.
- 15. Parmar, N., Chandrakar, P., Vishwakarma, P., Singh, K., Mitra, K., and Kar, S. (2018). Leishmania donovani exploits Tollip, a multitasking protein, to impair TLR/IL-1R signaling for its survival in the host. J. Immunol. 201, 957-970. https://doi.org/10.4049/jimmunol.1800062.
- 16. Xiong, W., Tang, T.X., Littleton, E., Karcini, A., Lazar, I.M., and Capelluto, D.G.S. (2019). Preferential phosphatidylinositol 5-phosphate binding contributes to a destabilization of the VHS domain structure of Tom1. Sci. Rep. 9, 10868. https://doi.org/10.1038/s41598-019-47386-z.
- 17. Prag, G., Lee, S., Mattera, R., Arighi, C.N., Beach, B.M., Bonifacino, J.S., and Hurley, J.H. (2005). Structural mechanism for ubiquitinated-cargo recognition by the Golgi-localized, gamma-ear-containing, ADP-ribosylation-factor-binding proteins. Proc. Natl. Acad. Sci. USA 102, 2334-2339. https://doi.org/10.1073/pnas.0500118102.
- 18. Hong, Y.H., Ahn, H.C., Lim, J., Kim, H.M., Ji, H.Y., Lee, S., Kim, J.H., Park, E.Y., Song, H.K., and Lee, B.J. (2009). Identification of a novel ubiquitin binding site of STAM1 VHS domain by NMR spectroscopy. FEBS Lett. 583, 287-292. https://doi.org/10.1016/j.febslet.2008.12.034.
- 19. Dephoure, N., Zhou, C., Villén, J., Beausoleil, S.A., Bakalarski, C.E., Elledge, S.J., and Gygi, S.P. (2008). A quantitative atlas of mitotic phosphorylation. Proc. Natl. Acad. Sci. USA 105, 10762-10767. https://doi. org/10.1073/pnas.0805139105.
- 20. Ren, X., and Hurley, J.H. (2010). VHS domains of ESCRT-0 cooperate in high-avidity binding to polyubiquitinated cargo. EMBO J. 29, 1045-1054. https://doi.org/10.1038/emboj.2010.6.
- 21. Kirchhausen, T. (2002). Single-handed recognition of a sorting traffic motif by the GGA proteins. Nat. Struct. Biol. 9, 241-244. https://doi.org/10.
- 22. Archuleta, T.L., Frazier, M.N., Monken, A.E., Kendall, A.K., Harp, J., McCoy, A.J., Creanza, N., and Jackson, L.P. (2017). Structure and evolution of ENTH and VHS/ENTH-like domains in tepsin. Traffic 18, 590-603. https://doi.org/10.1111/tra.12499
- 23. Herianto, S., Rathod, J., Shah, P., Chen, Y.Z., Wu, W.S., Liang, B., and Chen, C.S. (2021). Systematic analysis of phosphatidylinositol-5-phosphate-interacting proteins using yeast proteome microarrays. Anal. Chem. 93, 868-877. https://doi.org/10.1021/acs.analchem.0c03463.
- 24. Ellena, J.F., Xiong, W., Zhao, X., Shanaiah, N., and Capelluto, D.G.S. (2017). Backbone 1H, 15N, and 13C resonance assignments of the Tom1 VHS domain. Biomol. NMR Assign. 11, 1-4. https://doi.org/10. 1007/s12104-016-9709-4.
- 25. Cheever, M.L., Sato, T.K., de Beer, T., Kutateladze, T.G., Emr, S.D., and Overduin, M. (2001). Phox domain interaction with PtdIns(3)P targets the Vam7 t-SNARE to vacuole membranes. Nat. Cell Biol. 3, 613-618. https://doi.org/10.1038/35083000.

Structure

Article



- Tripathi-Giesgen, I., Behrends, C., and Alpi, A.F. (2021). The ubiquitin ligation machinery in the defense against bacterial pathogens. EMBO Rep. 22, e52864. https://doi.org/10.15252/embr.202152864.
- Mitra, S., Traughber, C.A., Brannon, M.K., Gomez, S., and Capelluto, D.G.S. (2013). Ubiquitin interacts with the Tollip C2 and CUE domains and inhibits binding of Tollip to phosphoinositides. J. Biol. Chem. 288, 25780–25791. https://doi.org/10.1074/jbc.M113.484170.
- Ankem, G., Mitra, S., Sun, F., Moreno, A.C., Chutvirasakul, B., Azurmendi, H.F., Li, L., and Capelluto, D.G.S. (2011). The C2 domain of Tollip, a Toll-like receptor signalling regulator, exhibits broad preference for phosphoinositides. Biochem. J. 435, 597–608. https://doi.org/10.1042/ BJ20102160.
- Puertollano, R., and Bonifacino, J.S. (2004). Interactions of GGA3 with the ubiquitin sorting machinery. Nat. Cell Biol. 6, 244–251. https://doi.org/10. 1038/ncb1106.
- Song, A.X., Zhou, C.J., Peng, Y., Gao, X.C., Zhou, Z.R., Fu, Q.S., Hong, J., Lin, D.H., and Hu, H.Y. (2010). Structural transformation of the tandem ubiquitin-interacting motifs in ataxin-3 and their cooperative interactions with ubiquitin chains. PLoS One 5, e13202. https://doi.org/10.1371/journal.pone.0013202
- Swanson, K.A., Kang, R.S., Stamenova, S.D., Hicke, L., and Radhakrishnan, I. (2003). Solution structure of Vps27 UIM-ubiquitin complex important for endosomal sorting and receptor downregulation. EMBO J. 22, 4597–4606. https://doi.org/10.1093/emboj/cdg471.
- Misra, S., Puertollano, R., Kato, Y., Bonifacino, J.S., and Hurley, J.H. (2002). Structural basis for acidic-cluster-dileucine sorting-signal recognition by VHS domains. Nature 415, 933–937. https://doi.org/10.1038/415933a.
- Cramer, J.F., Gustafsen, C., Behrens, M.A., Oliveira, C.L.P., Pedersen, J.S., Madsen, P., Petersen, C.M., and Thirup, S.S. (2010). GGA autoinhibition revisited. Traffic 11, 259–273. https://doi.org/10.1111/j.1600-0854. 2009.01017.x.
- Doray, B., Misra, S., Qian, Y., Brett, T.J., and Kornfeld, S. (2012). Do GGA adaptors bind internal DXXLL motifs? Traffic 13, 1315–1325. https://doi.org/10.1111/j.1600-0854.2012.01396.x.
- Li, X., Goobie, G.C., and Zhang, Y. (2021). Toll-interacting protein impacts on inflammation, autophagy, and vacuole trafficking in human disease.
 J. Mol. Med. 99, 21–31. https://doi.org/10.1007/s00109-020-01999-4.
- Misra, S., Beach, B.M., and Hurley, J.H. (2000). Structure of the VHS domain of human Tom1 (target of myb 1): insights into interactions with proteins and membranes. Biochemistry 39, 11282–11290.
- Wang, T., Liu, N.S., Seet, L.F., and Hong, W. (2010). The emerging role of VHS domain-containing Tom1, Tom1L1 and Tom1L2 in membrane trafficking. Traffic 11, 1119–1128. https://doi.org/10.1111/j.1600-0854.2010. 01098.x.
- Ko, M., Quiñones-Hinojosa, A., and Rao, R. (2020). Emerging links between endosomal pH and cancer. Cancer Metastasis Rev. 39, 519–534. https://doi.org/10.1007/s10555-020-09870-1.
- Morgan, A.J., Platt, F.M., Lloyd-Evans, E., and Galione, A. (2011).
 Molecular mechanisms of endolysosomal Ca2+ signalling in health and disease. Biochem. J. 439, 349–374. https://doi.org/10.1042/BJ20110949.
- Aharonovitz, O., Zaun, H.C., Balla, T., York, J.D., Orlowski, J., and Grinstein, S. (2000). Intracellular pH regulation by Na(+)/H(+) exchange requires phosphatidylinositol 4,5-bisphosphate. J. Cell Biol. 150, 213–224. https://doi.org/10.1083/jcb.150.1.213.
- Hendus-Altenburger, R., Vogensen, J., Pedersen, E.S., Luchini, A., Araya-Secchi, R., Bendsoe, A.H., Prasad, N.S., Prestel, A., Cardenas, M., Pedraz-Cuesta, E., et al. (2020). The intracellular lipid-binding domain of human Na(+)/H(+) exchanger 1 forms a lipid-protein co-structure essential for activity. Commun. Biol. 3, 731. https://doi.org/10.1038/s42003-020-01455-6
- Mitsui, K., Koshimura, Y., Yoshikawa, Y., Matsushita, M., and Kanazawa, H. (2011). The endosomal Na(+)/H(+) exchanger contributes to multivesicular body formation by regulating the recruitment of ESCRT-0 Vps27p to

- the endosomal membrane. J. Biol. Chem. 286, 37625–37638. https://doi.org/10.1074/jbc.M111.260612.
- Kojima, K., Amano, Y., Yoshino, K., Tanaka, N., Sugamura, K., and Takeshita, T. (2014). ESCRT-0 protein hepatocyte growth factor-regulated tyrosine kinase substrate (Hrs) is targeted to endosomes independently of signal-transducing adaptor molecule (STAM) and the complex formation with STAM promotes its endosomal dissociation. J. Biol. Chem. 289, 33296–33310. https://doi.org/10.1074/jbc.M114.578245.
- Lee, S.A., Eyeson, R., Cheever, M.L., Geng, J., Verkhusha, V.V., Burd, C., Overduin, M., and Kutateladze, T.G. (2005). Targeting of the FYVE domain to endosomal membranes is regulated by a histidine switch. Proc. Natl. Acad. Sci. USA 102, 13052–13057. https://doi.org/10.1073/pnas. 0503900102.
- He, J., Vora, M., Haney, R.M., Filonov, G.S., Musselman, C.A., Burd, C.G., Kutateladze, A.G., Verkhusha, V.V., Stahelin, R.V., and Kutateladze, T.G. (2009). Membrane insertion of the FYVE domain is modulated by pH. Proteins 76, 852–860. https://doi.org/10.1002/prot.22392.
- Owusu Kwarteng, D., Putta, P., and Kooijman, E.E. (2021). Ionization properties of monophosphoinositides in mixed model membranes. Biochim. Biophys. Acta. Biomembr. 1863, 183692. https://doi.org/10.1016/j.bba-mem.2021.183692.
- Vijay-Kumar, S., Bugg, C.E., and Cook, W.J. (1987). Structure of ubiquitin refined at 1.8 A resolution. J. Mol. Biol. 194, 531–544. https://doi.org/10. 1016/0022-2836(87)90679-6.
- Jaravine, V.A., Zhuravleva, A.V., Permi, P., Ibraghimov, I., and Orekhov, V.Y. (2008). Hyperdimensional NMR spectroscopy with nonlinear sampling. J. Am. Chem. Soc. 130, 3927–3936. https://doi.org/10.1021/ ja0772820.
- Abraham, M.J., Murtola, T., Schulz R, Páll, S., Smith, J.C., Hess, B., and Lindahl, E. (2015). High performance molecular simulations through multi-level parallelism from laptops to supercomputers. SoftwareX 1–2, 19–25. https://doi.org/10.1016/j.softx.2015.06.001.
- Páll S.A. M.J., Kutzner C., Hess B., Lindahl E. Tackling exascale software challenges in molecular dynamics simulations with GROMACS. In: Markidis S., Laure E., editors. Solving software challenges for exascale: International Conference on Exascale Applications and Software, EASC 2014, April 2-3, 2014, Revised Selected Papers. Springer; 2015. p. 3–27. https://doi/10.48550/arXiv.1506.00716
- Ramachandran, G.N., Ramakrishnan, C., and Sasisekharan, V. (1963).
 Stereochemistry of polypeptide chain configurations. J. Mol. Biol. 7, 95–99. https://doi.org/10.1016/s0022-2836(63)80023-6.
- Bowie, J.U., Lüthy, R., and Eisenberg, D. (1991). A method to identify protein sequences that fold into a known three-dimensional structure.
 Science 253, 164–170. https://doi.org/10.1126/science.1853201.
- Gautier, A., Mott, H.R., Bostock, M.J., Kirkpatrick, J.P., and Nietlispach, D. (2010). Structure determination of the seven-helix transmembrane receptor sensory rhodopsin II by solution NMR spectroscopy. Nat. Struct. Mol. Biol. 17, 768–774. https://doi.org/10.1038/nsmb.1807.
- Luthy, R., Bowie, J.U., and Eisenberg, D. (1992). Assessment of protein models with three-dimensional profiles. Nature 356, 83–85. https://doi. org/10.1038/356083a0.
- Jumper, J., Evans, R., Pritzel, A., Green, T., Figurnov, M., Ronneberger, O., Tunyasuvunakool, K., Bates, R., Žídek, A., Potapenko, A., et al. (2021). Highly accurate protein structure prediction with AlphaFold. Nature 596, 583–589. https://doi.org/10.1038/s41586-021-03819-2.
- Lee, W., Tonelli, M., and Markley, J.L. (2015). NMRFAM-SPARKY: enhanced software for biomolecular NMR spectroscopy. Bioinformatics 31, 1325–1327. https://doi.org/10.1093/bioinformatics/btu830.
- Baek, M., DiMaio, F., Anishchenko, I., Dauparas, J., Ovchinnikov, S., Lee, G.R., Wang, J., Cong, Q., Kinch, L.N., Schaeffer, R.D., et al. (2021). Accurate prediction of protein structures and interactions using a three-track neural network. Science 373, 871–876. https://doi.org/10.1126/science.abj8754.





- O'Leary, N.A., Wright, M.W., Brister, J.R., Ciufo, S., Haddad, D., McVeigh, R., Rajput, B., Robbertse, B., Smith-White, B., Ako-Adjei, D., et al. (2016).
 Reference sequence (RefSeq) database at NCBI: current status, taxonomic expansion, and functional annotation. Nucleic Acids Res. 44, D733–D745. https://doi.org/10.1093/nar/gkv1189.
- Wiederstein, M., and Sippl, M.J. (2007). ProSA-web: interactive web service for the recognition of errors in three-dimensional structures of proteins. Nucleic Acids Res. 35, W407–W410. https://doi.org/10.1093/nar/qkm290.
- Benkert, P., Biasini, M., and Schwede, T. (2011). Toward the estimation of the absolute quality of individual protein structure models. Bioinformatics 27, 343–350. https://doi.org/10.1093/bioinformatics/btq662.
- Williams, C.J., Headd, J.J., Moriarty, N.W., Prisant, M.G., Videau, L.L., Deis, L.N., Verma, V., Keedy, D.A., Hintze, B.J., Chen, V.B., et al. (2018). MolProbity: More and better reference data for improved all-atom structure validation. Protein Sci. 27, 293–315. https://doi.org/10.1002/pro.3330.
- Studer, G., Rempfer, C., Waterhouse, A.M., Gumienny, R., Haas, J., and Schwede, T. (2020). QMEANDisCo-distance constraints applied on model quality estimation. Bioinformatics 36, 1765–1771. https://doi.org/10.1093/ bioinformatics/btz828.
- Huang, J., Rauscher, S., Nawrocki, G., Ran, T., Feig, M., de Groot, B.L., Grubmüller, H., and MacKerell, A.D., Jr. (2017). CHARMM36m: an improved force field for folded and intrinsically disordered proteins. Nat. Methods 14, 71–73. https://doi.org/10.1038/nmeth.4067.
- Durell, S.R., Brooks, B.R., and Ben-Naim, A. (1994). Solvent-induced forces between 2 hydrophilic groups. J. Phys. Chem. 98, 2198–2202. https://doi.org/10.1021/j100059a038.
- Jorgensen, W.L., Chandrasekhar, J., Madura, J.D., Impey, R.W., and Klein, M.L. (1983). Comparison of simple potential functions for simulating liquid water. J. Chem. Phys. 79, 926–935. https://doi.org/10.1063/1. 445869.

- Debye, P. (1909). Approximation formula for cylindrical function in high value arguments and alterable index values. Math. Ann. 67, 535–558. https://doi.org/10.1007/Bf01450097.
- Berendsen, H.J.C., Postma, J.P.M., Vangunsteren, W.F., Dinola, A., and Haak, J.R. (1984). Molecular-dynamics with coupling to an external bath. J. Chem. Phys. 81, 3684–3690. https://doi.org/10.1063/1.448118.
- Darden, T., York, D., and Pedersen, L. (1993). Particle mesh Ewald an N.Log(N) method for Ewald sums in large systems. J. Chem. Phys. 98, 10089–10092. https://doi.org/10.1063/1.464397.
- Essmann, U., Perera, L., Berkowitz, M.L., Darden, T., Lee, H., and Pedersen, L.G. (1995). A smooth particle mesh Ewald method. J. Chem. Phys. 103, 8577–8593. https://doi.org/10.1063/1.470117.
- Hess, B. (2008). P-LINCS: A parallel linear constraint solver for molecular simulation. J. Chem. Theory Comput. 4, 116–122. https://doi.org/10.1021/ ct700200b.
- Nose, S. (1984). A molecular-dynamics method for simulations in the canonical ensemble. Mol. Phys. 52, 255–268. https://doi.org/10.1080/00268978400101201.
- Parrinello, M., and Rahman, A. (1981). Polymorphic transitions in singlecrystals - a new molecular-dynamics method. J. Appl. Phys. 52, 7182– 7190. https://doi.org/10.1063/1.328693.
- Páll, S., and Hess, B. (2013). A flexible algorithm for calculating pair interactions on SIMD architectures. Comput. Phys. Commun. 184, 2641–2650. https://doi.org/10.1016/j.cpc.2013.06.003.
- 74. Schrödinger Release 2023-3: BioLuminate, Schrödinger, LLC, 2024.
- Schrödinger, L. (2023). The PyMOL Molecular Graphics System, Version 2.5.4 (Schrödinger, LLC).
- De Mol, N., and Fisher, M. (2010). Kinetic and thermodynamic analysis of ligand-receptor interactions: SPR applications in drug development. In Surface Plasmon Resonance: Methods and Protocols (Methods in Molecular Biology). Chapter 5, 123–171. https://doi/10.1039/ 9781847558220-0012.

Structure Article



STAR***METHODS**

KEY RESOURCES TABLE

REAGENT or RESOURCE	SOURCE	IDENTIFIER
Bacterial and virus strains		
E. cloni® 10G	Biosearch Technologies	Cat# 60107-1
Escherichia coli Rosetta	Novagen/Sigma-Aldrich	Cat# 70953
Escherichia coli Rosetta (DE3)	Novagen/Sigma-Aldrich	Cat# 70954
Chemicals, peptides, and recombinant proteins		
1,2-dioleoyl-sn-glycero-3-phosphocholine	AVANTI Lipids	Cat#850375
1,2-dioleoyl-sn-glycero-3-phosphoethanolamine	AVANTI Lipids	Cat#850725C
30% Acrylamide/Bis solution, 19:1	BioRad	Cat#1610156
Ammonium chloride ¹⁵ N	Cambridge Isotope Laboratories, Inc.	Cat#NLM-467
Benzamidine	Research Products International Corp.	Cat#B12000
Bis-sulfosuccinimidyl substrate	ThermoScientific	Cat#21580
Citric acid (D4)	Cambridge Isotope Laboratories	Cat#DLM-3487
Deuterium oxide	Cambridge Isotope Laboratories, Inc.	Cat#DLM-4
Dibutanoyl PtdIns5P	Echelon Biosciences	Cat#P-5004
Dipalmitoyl PtdIns3P	Echelon Biosciences	Cat#P-3016
Dipalmitoyl PtdIns5P	Echelon Biosciences	Cat#P-5016
DL-1,4-Dithiothreitol (D10)	Cambridge Isotope Laboratories, Inc.	Cat#DLM-2622
DL-dithiothreitol, Cleland's Reagent	GoldBio	Cat#DTT50
DXXLL peptide (EFPMT <u>DLDML</u> SPIHTPQRTV)	Biomatik	
Glutaraldehyde	MP Biologicals	Cat#198595
Glutathione agarose resin	GoldBio	Cat#G-250
His60 Ni Superflow resin	TaKaRa	Cat# 635662
midazole	Acros Organics	Cat#301872500
sopropyl-β-D-thiogalactopryanoside	Chem-Impex Int'l Inc.	Cat#00194
Lysozyme	Sigma-Aldrich	Cat#L6876
pET28a	Sigma-Aldrich	Cat#69864
pGEX4T3	Cytiva	Cat#28954552
oGEX6P1	Cytiva	Cat#28954648
Reduced glutathione	BioBasic	Cat#GB0229
Thrombin	MP Biomedicals	Cat#154163
Tris (D11)	Cambridge Isotope Laboratories, Inc.	Cat#DLM-1814
Triton X-100	MP Biomedicals	Cat#04807426-CF
Trypsin	Millipore Sigma	Cat#T6567
Tween 20	MP Biomedicals	Cat#500-018-3
Critical commercial assays		
BCA Protein Assay Kit	Pierce, ThermoScientific	Cat#23227
Deposited data		
Human TOM1 sequence	Yamakami et al. ⁵	National Center for Biotechnology Information NM_001135732.2
Human Ubiquitin structure	Vijay-Kumar et al. ⁴⁷	Protein DataBank: 1UBQ
Software and algorithms		
AlphaFold	Jumper et al. ⁴⁸	https://alphafold.ebi.ac.uk
CHARMM36m forcefield	Huang et al. ⁴⁹	https://academiccharmm.org
	Durell ⁵⁰	https://academiccharmm.org

(Continued on next page)





Continued		
REAGENT or RESOURCE	SOURCE	IDENTIFIER
Excel v16.83	Microsoft	https://www.microsoft.com/ en-us/microsoft-365/excel
GROMACS 2020.4	Abraham et al. ⁵¹	https://www.gromacs.org/
GROMACS analysis package	Maestro	https://www.gromacs.org/
Illustrator v28.3	Adobe	https://www.adobe.com
ImageJ		https://imagej.nih.gov/ij/
ImageLab	BioRad	https://www.bio-rad.com
MicroCal PEAQ-ITC analysis software	Malvern Panalytical	https://www.malvernpanalytical.com
Mnova 14.0.0	MestreLab	https://mestrelab.com
ProSA	Wiederstein et al. ⁵²	https://www.hsls.pitt.edu
PyMOL 2.5.4.	Schrödinger	https://pymol.org
Robetta	Baek et al. ⁵³	https://robetta.bakerlab.org
Schrödinger Maestro 13.9	Schrödinger	https://www.schrodinger.com
Sparky	Lee et al. ⁴⁵	https://www.cgl.ucsf.edu/home/sparky/
Spectra Analysis Software (CD)	Jasco	https://jascoinc.com
Swiss-Model	Benkert et al. ⁵⁴	https://swissmodel.expasy.org/
Unicorn 5.11	Cytiva Life Sciences	https://www.cytivalifesciences.com
Verify3D	Bower et al. ⁵⁵	https://www.doe-mbi.ucla.edu/verify3d/
Other		
200-nm polycarbonate membrane	Cytiva, Whatman Nuclepore	Cat#10417004
HiLoad 16/600 Superdex 200	Cytiva Life Sciences	Cat#28-9893-35
HiLoad 16/600 Superdex 75	Cytiva Life Sciences	Cat#28-9893-33
NiD200M chip	Xantec	Cat#SCB NiD200M

RESOURCE AVAILABILITY

Lead contact

Further information and requests for resources and reagents should be directed to and will be fulfilled by the lead contact, Daniel G. S. Capelluto (capellut@vt.edu).

Materials availability

All plasmids used in this study will be made available upon request. The study did not generate other new or unique reagents.

Data and code availability

- All data reported in this paper will be shared by the lead contact upon request. Full SDS-PAGE gel images are available in this
 paper's supplemental information (Figures S8, S9, S12, and S17).
- This paper does not report original code.
- Any additional information required to reanalyze the data reported in this paper is available from the lead contact upon request.

EXPERIMENTAL MODEL AND STUDY PARTICIPANT DETAILS

The following bacterial strain was used in this study: Escherichia coli Rosetta strain.

METHOD DETAILS

Cloning and mutagenesis

The cDNA construct expressing human TOM1 VHS domain (residues 11–149), TOM1 VHS-DXXLL (residues 11–169), and Vam7p PX domain (residues 2–134) were cloned into pGEX4T3. Constructs expressing human TOM1,⁶ TOM1 ΔCTD (residues 1–309), TOM1 GAT (residues 215–309), TOM1 linker-GAT (150–309), and human TOLLIP⁶ were cloned into pGEX6P1. TOM1 was also cloned into a pET28a vector.⁶ Human ubiquitin, cloned into pET24d was a gift from Dr. Julie Forman-Kay, University of Toronto. PCR-based site-directed mutagenesis was introduced into TOM1 and TOM1 VHS constructs. The list of primers used in this study is shown in Table S3.

Structure Article



Protein expression and purification

Proteins were expressed in an Escherichia coli Rosetta strain. The GST-tagged proteins (TOM1, truncated forms of TOM1, TOM1 domains and related mutations, and TOLLIP), His-tagged proteins (TOM1 and ubiquitin), and the uniformly ¹⁵N-labeled TOM1 constructs and ubiquitin were overexpressed and purified as previously reported. 24,27 Cell pellets were harvested and lysed by the addition of 0.1 mg/mL lysozyme and 0.1% Triton X-100 in a buffer containing 50 mM Tris-HCl (pH 7.3), 500 mM NaCl, 1 mM 1,4-dithiothreitol, and 5 mM benzamidine. The lysate further underwent sonication and centrifugation. The resultant supernatant was collected and incubated with glutathione affinity beads (for GST-tagged proteins; Gold Biotechnology) or Ni-NTA beads (for His-tagged proteins; Clontech). Fusion proteins were eluted off the beads by the addition of either 100 mM reduced glutathione, pH 7 (for GSTtagged proteins) or 500 mM imidazole, pH 8 (for His-tagged proteins). When required, His tags were removed by addition of tobacco etch virus protease (substrate to protease w:w = 10:1), whereas GST tags were removed using 200 units of thrombin/L culture, overnight at 4°C (for constructs cloned into pGEX4T3) or HRV-3C protease (200 μg/L culture) overnight at 4°C (for constructs cloned into pGEX6P1). Removal of protein aggregates or degradation products was achieved by an additional purification step using size-exclusion chromatography columns driven by an ÄKTA Pure FPLC system (Cytiva). Protein concentrations were determined with corresponding extinction coefficients at the absorbance of 280 nm using NanoDrop (Thermo Scientific, USA). In the case of ubiquitin and the TOM1 GAT domain, both of which lack aromatic residues, the concentrations were determined using the extinction coefficients of 1280 M⁻¹mm⁻¹ at 280 nm (ubiquitin) and 13,301.8 M⁻¹mm⁻¹ at 214 nm (TOM1 GAT) using NanoDrop and bicinchoninic acid (BCA) assay following manufacturers protocol (Pierce, Thermo Fisher). The DXXLL peptide (TOM1 residues 150-EFPMTDLDML SPIHTPQRTV-169) was synthesized as HCl salt form (Biomatik).

Isothermal titration calorimetry

ITC measurements were carried out using a MicroCal PEAQ (Malvern). Proteins were prepared in 20 mM HEPES (pH 7.3) and 150 mM KCl or 20 mM citrate (pH 5.0) and 150 mM KCl. Ligand was placed in the syringe at a concentration of 5 mM (pH 7.3) or 1 mM (pH 5.0), whereas the protein was placed in the cell at a concentration of 50 μ M (pH 7.3) or 10 μ M (pH 5.0). The experiments were carried out at 25°C with 13 injections of 3 μ L each, and reference power of 10 μ cal. Measurements were carried out at least in duplicate. The reported heats of binding were established by integrating the experimental peaks after adjusting the effect of heat dilution of ligands into buffer in a control measurement. The integrated heat data were analyzed with MicroCal PEAQ-ITC analysis software.

NMR spectroscopy

NMR experiments were performed on a Bruker Avance III 600 MHz equipped with a TCI Prodigy probe at 25°C. An HSQC of ¹⁵N-labeled indicated proteins (100 μM) was collected in the absence and presence of the indicated unlabeled ligands. NMR chemical shifts changes were analyzed using Sparky⁵⁶ and the spectra images were processed using Mnova. The normalized chemical shift perturbations, induced by ligands, were estimated using the following equation⁵³:

$$\Delta\delta(1_{H}, 15_{N}) = \left[(\Delta\delta1_{H})^{2} + (\Delta\delta15_{N})^{2} / 6 \right]^{0.5}$$
 Equation 1

The chemical shift positions have been mapped with the backbone¹ H,¹³ C, and¹⁵ N chemical shift assignments for human Ub (BMRB: 15410)⁴⁸ and for TOM1 VHS (BMRB: 26806).²⁴

Circular dichroism

CD structural analysis of the proteins was performed using a Jasco J-815 spectropolarimeter. Proteins were prepared in 5 mM sodium citrate (pH 7.3 and 5.0) and 50 mM kF. Five-accumulated far-UV CD measurements were acquired using 5–8 μ M protein in a 1-mm path length quartz cell using a bandwidth of 1-nm and a response time of 1 s, a D.I.T. of 0.5 s, and a scan speed of 50 nm/min from 190 to 260 nm. Five-accumulated near-UV CD spectra of protein (200–300 μ M) were acquired at 50 nm/min from 270 to 350 nm. In both cases, a scan of the buffer was subtracted from the corresponding averaged spectra. Near-UV data were further processed through smoothing using the Savitzky-Golay filter. All spectra were then converted to molar ellipticity units using Spectra Analysis software. For the comparison of TOM1 VHS to TOM1 VHS-DXXLL, conversion to mean residue ellipticity was performed to account for differences in molecular weights.

Limited trypsin proteolysis

Ten μg of TOM1 VHS (residues 11–149) or TOM1 VHS-DXXLL (residues 11–169) and varying concentrations of trypsin (0.040–0.625 $\mu g/\mu L$; Millipore Sigma) were incubated for 30 min at room temperature and the reaction quenched by adding SDS-PAGE loading buffer. Samples were loaded onto a 15% Acrylamide SDS-PAGE and analyzed using Bio-Rad ImageLab.

Molecular dynamics simulations

Multiple TOM1 models were created using Robetta⁵⁷ and AlphaFold.⁵⁵ The reference sequence of the protein was retrieved from the National Center for Biotechnology Information, accession number NM_001135732.2.⁵⁸ The top models from each method were validated and compared using Verify3D,^{52,54} ProSA,⁵⁹ and Swiss-Model structural assessments.^{51,60–62} The Robetta model of TOM1 was determined to be the best model and was used for subsequent simulation and analysis.





The GROMACS 2020.4^{49,50} software suite was used for all MD simulations. The CHARMM36m forcefield⁶³ and the CHARMM-modified TIP3P^{64,65} water model were applied. Two systems were built with residue and peptide termini protonated according to their canonical states at pH 5 and 7. The systems were built in a cubic box (2629 nm³) with a minimum solute-box distance of 1 nm and contained 150 mM KCl to achieve a net neutral charge and to mimic physiological conditions.

Energy minimization was performed with the steepest descent algorithm⁶⁶ with a maximum force constraint of 1000 kJ/mol nm. Three replicate systems at both pH 5 and 7 were individually equilibrated at constant volume and temperature (NVT), then constant pressure and temperature (NPT), while restraining heavy atoms. NVT equilibration used the modified Berendsen temperature coupling method⁶⁷ at a temperature of 298 K for 100 ps. Next, isothermal-isobaric conditions of 298 K and 1 bar were applied for 100 ps using the Berendsen pressure coupling method.⁶⁷

Atom restraints were removed, and periodic boundary conditions were applied to all MD simulations. A short-range cutoff of 1.2 nm was applied to all nonbonded interactions. Long-range interactions were calculated using the particle mesh Ewald (PME) method 68,69 using cubic interpolation and a Fourier grid spacing of 0.16 nm. An integration timestep of 2 fs was used along with the fourth order P-LINCS algorithm 70 to constrain all bonds. The modified Berendsen temperature coupling method, Parrinello–Rahman pressure coupling method 71,72 at 298 K and 1 bar respectively, and the Verlet cutoff scheme 73 were used for all production MD simulations. Periodic boundary conditions were employed. van der Waals forces were computed with the Lennard–Jones equation and smoothly switched to zero from 1.0 to 1.2 nm. After the initial production MD simulation, the six replicates were each extended to 1000 ns, for a total of 3 μ s of simulation time per pH.

Trajectories were analyzed with root-mean-square deviation (RMSD), root-mean-square fluctuation (RMSF), protein secondary structure (DSSP), solvent accessible surface area (SASA), density, volume, and free energy by using the GROMACS analysis package⁷⁴ and in-house scripts. A clustering analysis was conducted over the last 200 ns of the simulation using the Gromos algorithm with a rms cutoff of 0.3 nm.

The effects of phosphorylation on protein conformation were investigated by modifying S160 to phosphoserine (pS160) and T164 to phosphothreonine (pT164) using Schrödinger Maestro 13.9.⁷⁵ These modifications were introduced individually and simultaneously at pH 7. The structures were processed using the same NVT, NPT, energy minimization, and production simulations using GROMACS, without the extended simulation protocol applied to the initial replicates. RMSD analyses were conducted to compare the mutated structure with the processed structure.

Protein-protein docking of ubiquitin (PDB ID: 1UBQ)⁴⁷ to the TOM1 VHS-linker-GAT region of the dominant structure of each simulation was performed in Schrodinger Maestro 13.9 using PIPER. Ten thousand ubiquitin rotations were probed, and the 30 best docking poses were exported for analysis. The best poses were optimized, and binding energies were calculated in Schrodinger Maestro 13.9 using MM-GBSA. An interaction fingerprint analysis was performed to determine residues involved in binding.

Initial starting structures, dominant morphology structure files from simulation, and parameter files can be found on Open Science Framework (https://www.cos.io). Images of the protein were created with PyMOL 2.5.4.⁷⁵

Surface plasmon resonance

A Xantec NiD200M chip was employed to assess the binding of His-TOM1 or His-TOM1 S160D/T164D to TOLLIP on a Biacore X-100 system (Cytiva). A multi-cycle experiment was carried out following the Biacore kinetics/affinity assay workflow. Initially, the sensor chip was conditioned with 5 mM NiCl $_2$ in a buffer containing 10 mM HEPES (pH 7.0), 150 mM NaCl and supplemented with 50 μ M EDTA and 0.005% Tween 20. All proteins were prepared in the same buffer. Subsequently, each His-TOM1 protein was introduced to the chip at a concentration of 20 nM, followed by a wash cycle using 3 mM EDTA to remove excess of protein. Three start-up cycles with buffer alone were performed prior to testing TOLLIP at concentrations ranging from 1 to 30 nM, with each concentration tested in individual cycles. Each cycle concluded with a regeneration step employing 100 mM NaOH with a contact time of 180 s to restore the original baseline before the subsequent cycle. The resulting SPR traces were analyzed using a two-state reaction model. In this model, a protein binding event is measured by the equilibrium association constant K_b ($K_b = k_{a1}/k_{d1}$). Upon binding, the protein displays a structural change, which is estimated by the equilibrium constant K_{conf} [$K_{conf} = k_{a2}/k_{d2}$ and $K_a = K_b(1 + K_{conf}) = 1/K_D$].

Liposome co-sedimentation assay

Liposomes were composed of 1,2-dioleoyl-*sn*-glycero-3-phosphocholine (DOPC) and 1,2-dioleoyl-*sn*-glycero-3-phosphoethanolamine (DOPE) (Avanti Lipids) (70:30 ratio) with or without 20% dipalmitoyl PtdIns5P (Echelon Biosciences and Cayman Chemical). For Vam7p PX experiments, liposomes contained 10% dipalmitoyl PtdIns3P (Echelon Biosciences). DOPC and DOPE were dissolved in chloroform:methanol (1:1), whereas PtdIns5P and PtdIns3P were solubilized in chloroform:methanol:water (65:35:4). Lipid mixtures were dried under N₂ (g) to form a thin film and placed in a desiccator under vacuum for at least 2 h. Lipids were then resuspended in pre-warmed (60C) buffers with the following compositions: 20 mM Tris (pH 7.3) and 100 mM NaCl; 20 mM sodium citrate (pH 5.0, 5.2, 5.5, and 6.0) and 100 mM NaCl at a concentration of 2 mg/mL and allowed to hydrate for 1 h at 60°C. Lipid mixtures were vortexed every 10 min to avoid formation of clumps. After hydration, the liposomes were subjected to five freeze/thaw cycles using N₂ (L) and a water bath at 60°C. Liposomes were extruded through a mini-extruder (Avanti Polar Lipids) at 60°C using a 200-nm polycarbonate membrane (Whatman Nuclepore). Proteins were in 20 mM buffer, at appropriate pH, and 100 mM NaCl. Liposomes were mixed with 20 μg of the indicated protein and incubated for 1 h at room temperature. Suspensions were centrifuged for 1 h at 180,000xg at 20°C in an MLA-150 rotor using a Beckman Coulter Optima Max-XP. Resultant pellets were resuspended in the same volume of buffer as the original suspension. Samples were loaded on an SDS-PAGE and resultant Coomassie Blue stained

Structure Article



bands were imaged using a Bio-Rad GelDoc Go Imaging System and analyzed using ImageJ software. Error bars represent the standard deviation of at least three independent experiments.

Chemical crosslinking

Crosslinking experiments were performed using either bis-sulfosuccinimidyl substrate (BS, 3 Thermo Scientific) or glutaraldehyde (MP Biologicals). In each case, His-TOM1 and GST (6 μ g each) were prepared in a buffer containing 20 mM HEPES (pH 7.3) and 150 mM KCl. Proteins were then incubated with the respective crosslinkers at their specified concentrations for 30 min at room temperature, followed by the addition of 40 mM Tris for 15 min to quench the reactions. Samples were analyzed by SDS-PAGE. For the TOM1-TOLLIP complex, prior to the co-sedimentation assay, TOM1 and TOLLIP were co-purified as described previously and incubated with 5 mM BS 3 for 1.5 h on ice. The reaction was terminated by adding 25 mM Tris. Subsequently, the resulting protein solution was injected into a Superdex 200 column to purify the target complex from unwanted aggregates and monomers.

Analytical size-exclusion chromatography

Analytical size exclusion chromatography was conducted on purified samples with HiLoad 16/600 Superdex columns (Superdex 75 and 200) connected to an ÄKTA Pure unit with a continuous flow rate of 1 mL/min. Columns were calibrated with size-exclusion marker calibration kits, spanning the ranges of 1,355–150,000 Da (Superdex 75) and 12,384–480,000 Da (Superdex 200) (Sigma-Aldrich), to determine the apparent molecular masses of the observed species. The columns were equilibrated with 20 mM HEPES (pH 7.3) and 150 mM KCl or with 20 mM sodium citrate (pH 5.0) and 150 mM KCl. Each experiment was replicated at least twice.

Visualization

Figures were designed using Microsoft Excel v16.83 and Adobe Illustrator v28.3.

QUANTIFICATION AND STATISTICAL ANALYSIS

Statistical analyses were carried out using the two-tailed unpaired t-test for all liposome co-sedimentation assays. Summarized data were depicted in figures as mean \pm SD from at least two independent experiments. Statistical significance was established as ***p < 0.001, **p < 0.01, and *p < 0.05.

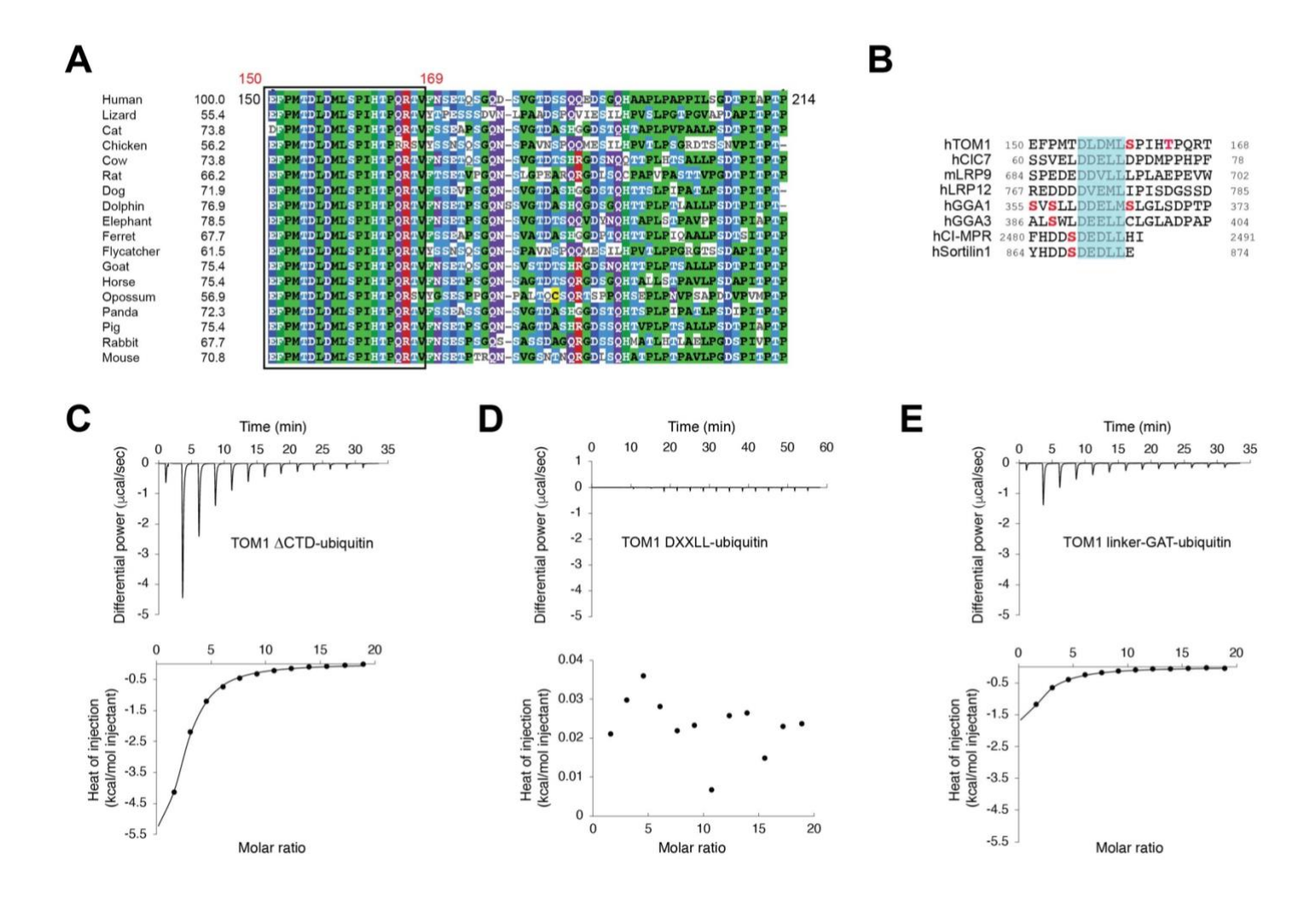
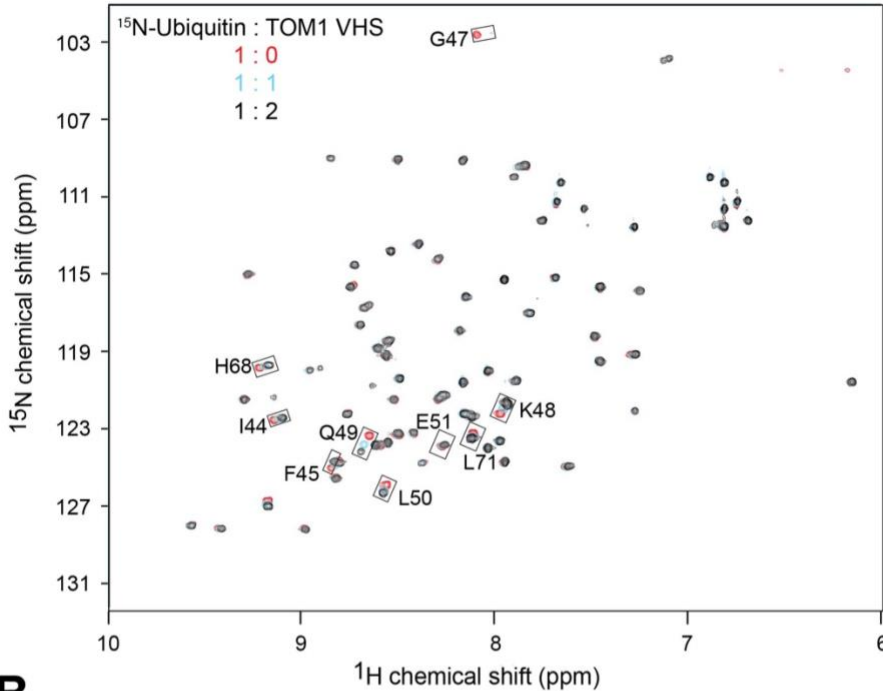


Figure S1. The function of the DXXLL-containing region in TOM1, related to Figures 1 and 2. (A) Sequence alignment of the linker region of TOM1 proteins from the indicated organisms. The highly conserved DXXLL regions (residues 150-169 in human TOM1) is highlighted with a black box. (B) Sequence alignment among proteins containing DXXLL motifs (shaded in blue) with the reported phosphorylation sites labeled in red. hCIC7, human chloride channel 7; mLRP9, mouse low-density lipoprotein receptor-related protein 9; hLRP12, human low-density lipoprotein receptor-related protein 12; hGGA, human Golgi-localized, gamma adaptin ear-containing, ARF-binding; hCI-MPR, human cation-independent mannose 6-phosphate receptor. (C-E) Calorimetric titration curves for the association of TOM1 Δ CTD (C), TOM1 DXXLL (D) and TOM1 linker-GAT (E) to ubiquitin. The upper and lower panels depict the heat change produced upon binding (µcal/sec), and the integrated binding heat change over the ligand/protein ratio (kcal/mol injectant). Bindings were subtracted with the heat of corresponding ligand to

buffer and best fit with a one set of sites binding model, with stoichiometry (N) fixed to either 1 or 2, depending upon the TOM1 construct tested.







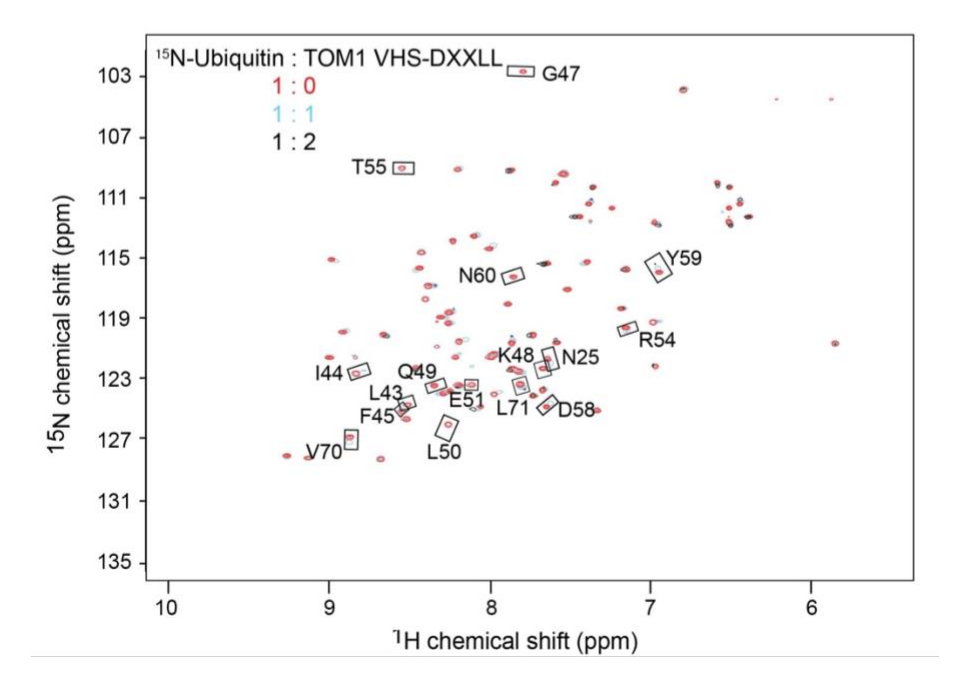


Figure S2. The TOM1 DXXLL region promotes additional contacts for the interaction of TOM1 VHS with ubiquitin, related to Figures 1 and 2. (A) Overlay of ¹H-¹⁵N HSQC spectra of ¹H-¹⁵N ubiquitin in the absence (red) and presence of 1- (cyan) and 2-fold (black) of TOM1 VHS. (**B**) Overlay of ¹H-¹⁵N HSQC spectra of ¹H-¹⁵N ubiquitin in the absence (red) and presence of 1- (cyan) and 2-fold (black) of TOM1 VHS-DXXLL. In both panels, chemical shifts undergoing perturbations are boxed and labeled with the corresponding residue.

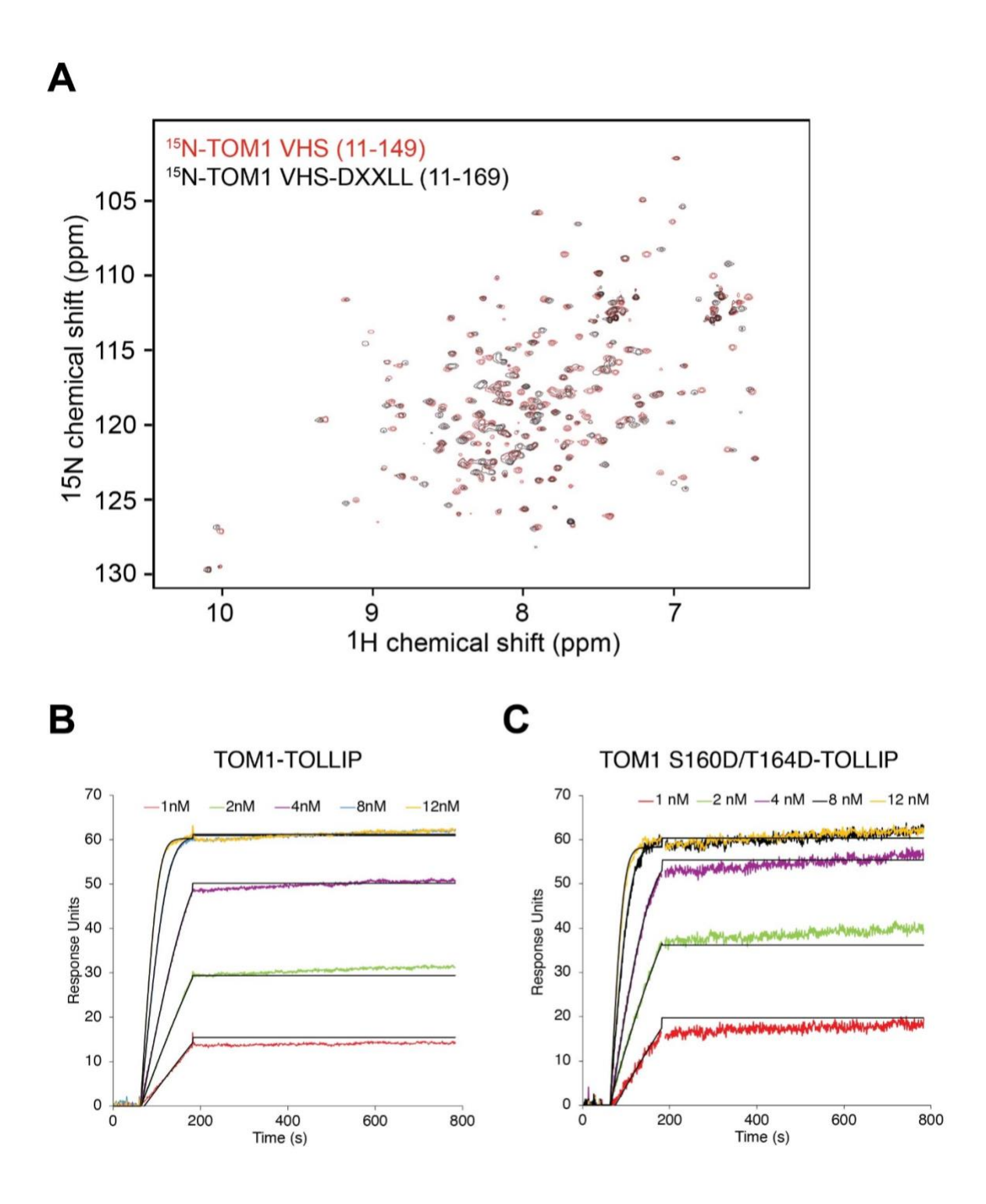
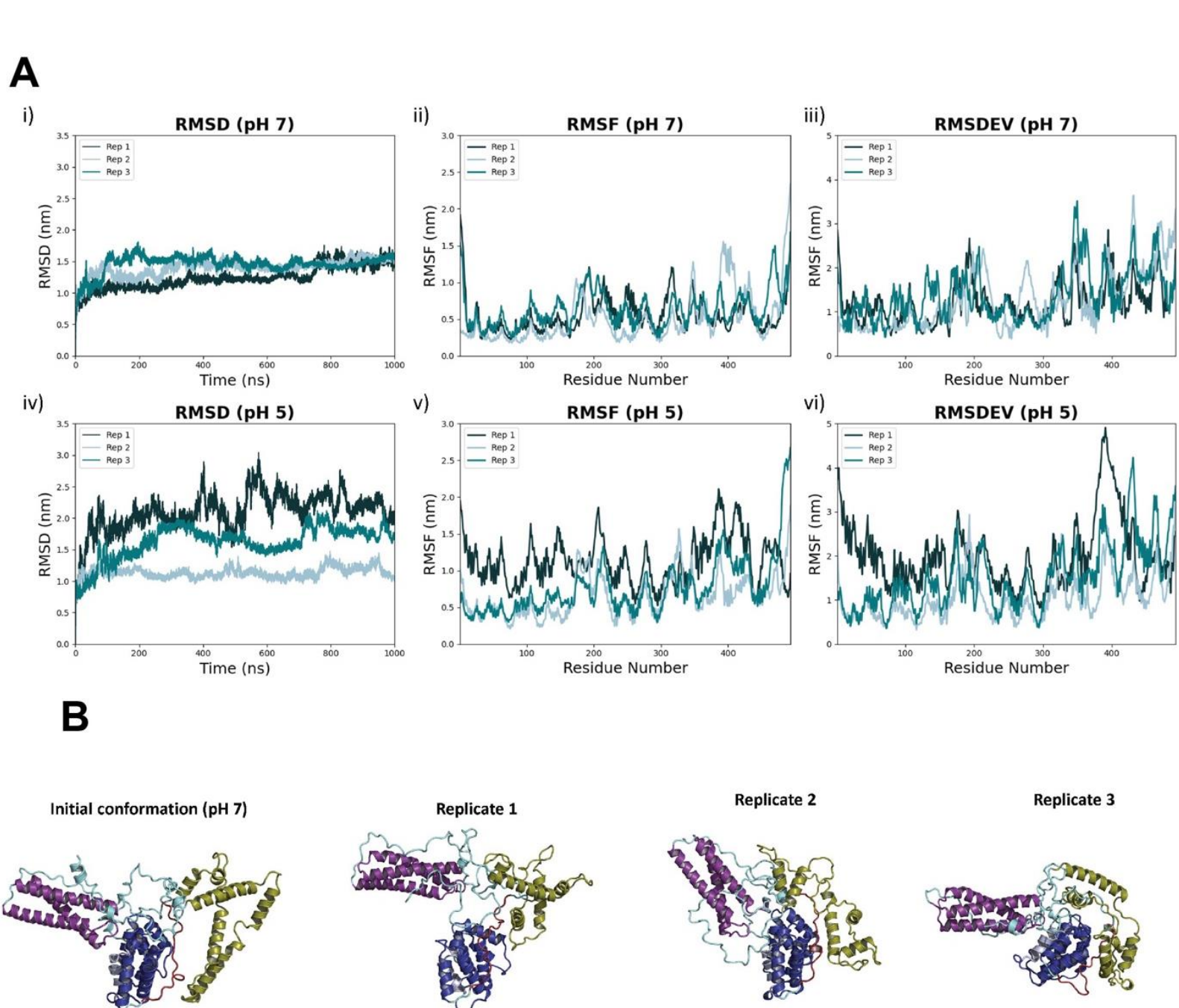
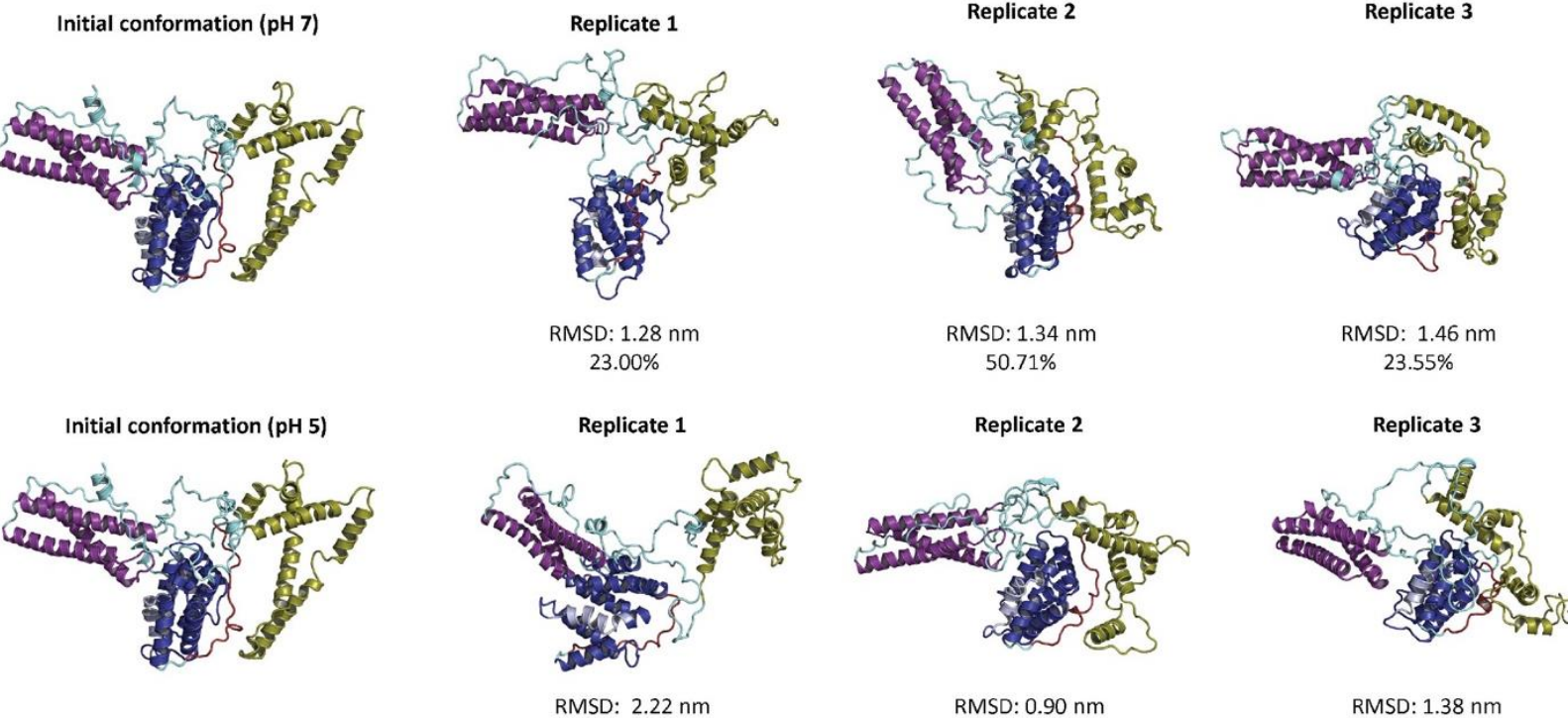


Figure S3. The DXXLL region promotes local conformational changes in the TOM1 VHS domain, related to Figures 1, 2, and 4. (A) Overlay of ¹H-¹⁵N HSQC spectra of ¹⁵N-TOM1 VHS (11-149; red) and ¹⁵N-TOM1 VHS-DXXLL (11-169; black). (**B-C**) SPR sensorgrams for the interaction of TOLLIP with TOM1 (**B**) and TOM1 S160D/T164D (**C**).





14.27%

14.35%

9.74%

Figure S4. Structural properties of TOM1 at pH 7 and 5, related to Figure 3. (**A**) Changes of the structure of TOM1 at pH 7 (top) and pH 5 (bottom) over time compared to initial structure. Left to right, root-mean-square deviation (RMSD) of backbone atoms; root-mean-square fluctuation (RMSF) for all atoms of TOM1 residues; root-mean-square deviation (RMSD) of TOM1 residues over time compared to initial structure. (**B**) Dominant morphology of TOM1 at pH 7 (top) and pH 5 (bottom). Representative dominant protein conformation of each replicate, determined by clustering the last 200 ns of the simulation with an RMS cutoff of 0.3 nm. Color codes are as follows: VHS domain: dark blue; DXXLL region: dark red; GAT domain: purple; PtdIns5P-binding site: light blue; CTD: yellow; non-domain loops: cyan.



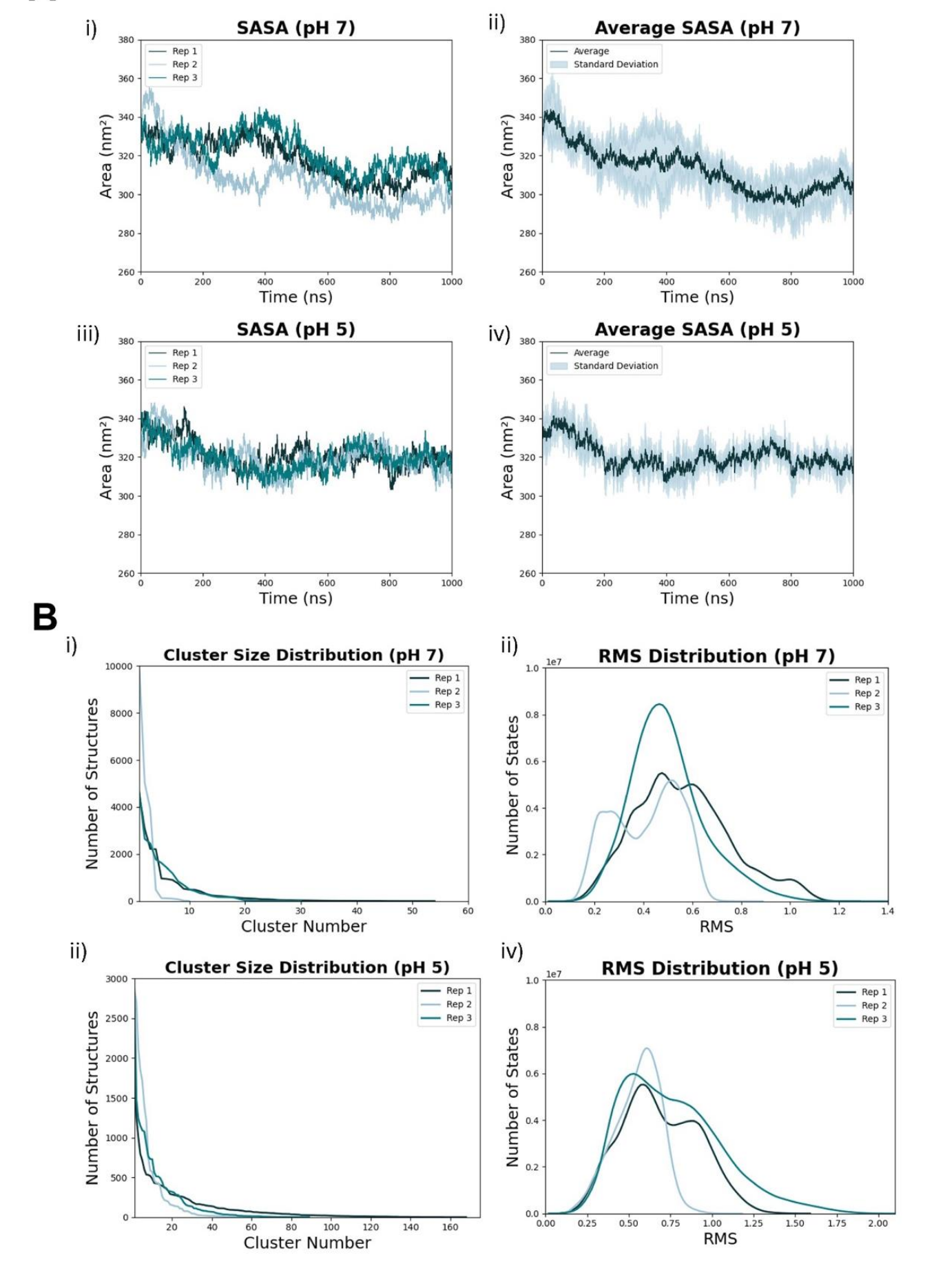
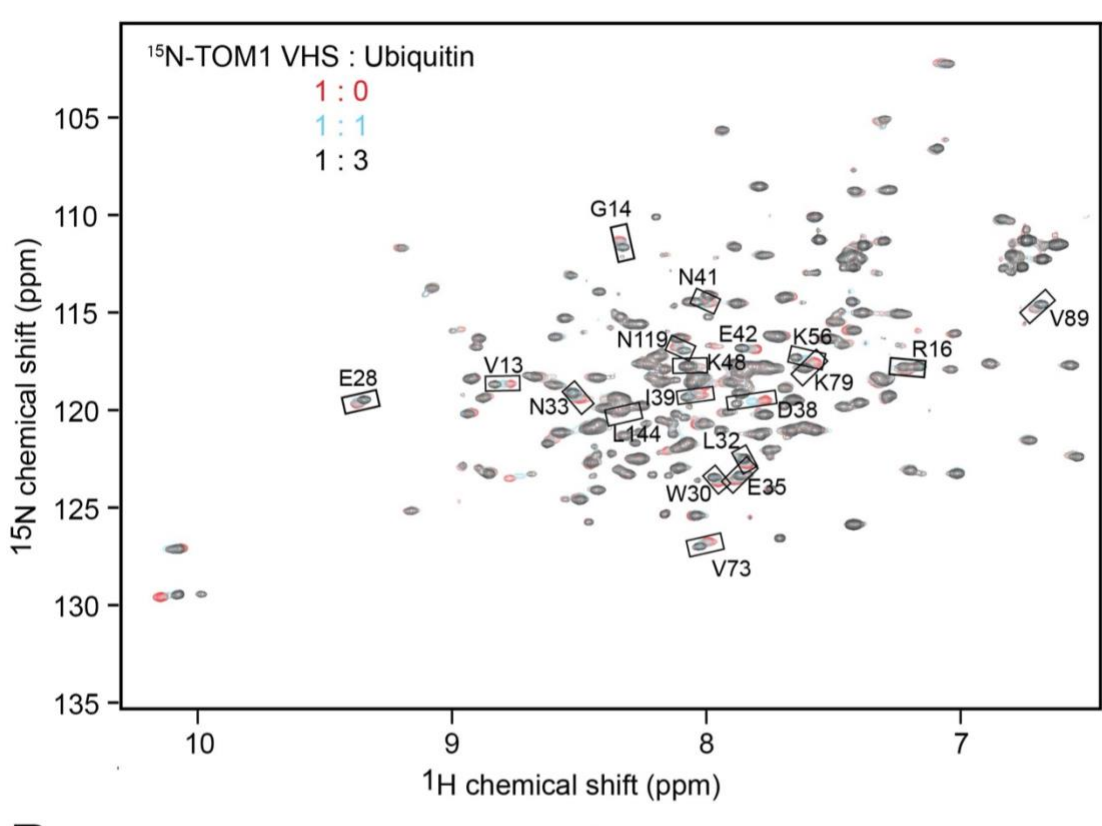


Figure S5. Additional properties of TOM1 at pH 7 and 5, related to Figure 3. (A) Solvent accessible surface area (SASA) of TOM1 at pH 7 (I) and pH 5 (III). The average solvent accessible surface area (nm²) of TOM1 replicates at pH 7 (II) and pH 5 (IV). (B) Clustering distributions of TOM1 structures at pH 7 (I) and pH 5 (III) at the last 200 ns of the simulation with an RMS cutoff of 0.3 nm. The RMS distribution of TOM1at pH 7 (II) and pH 5 (IV).





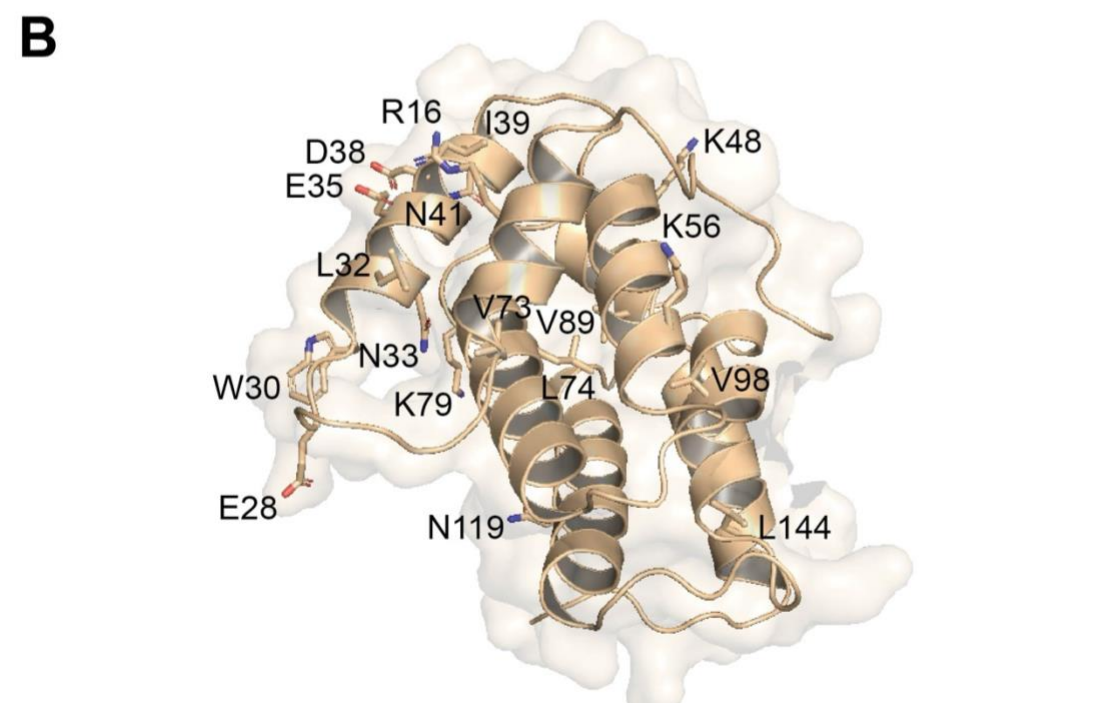
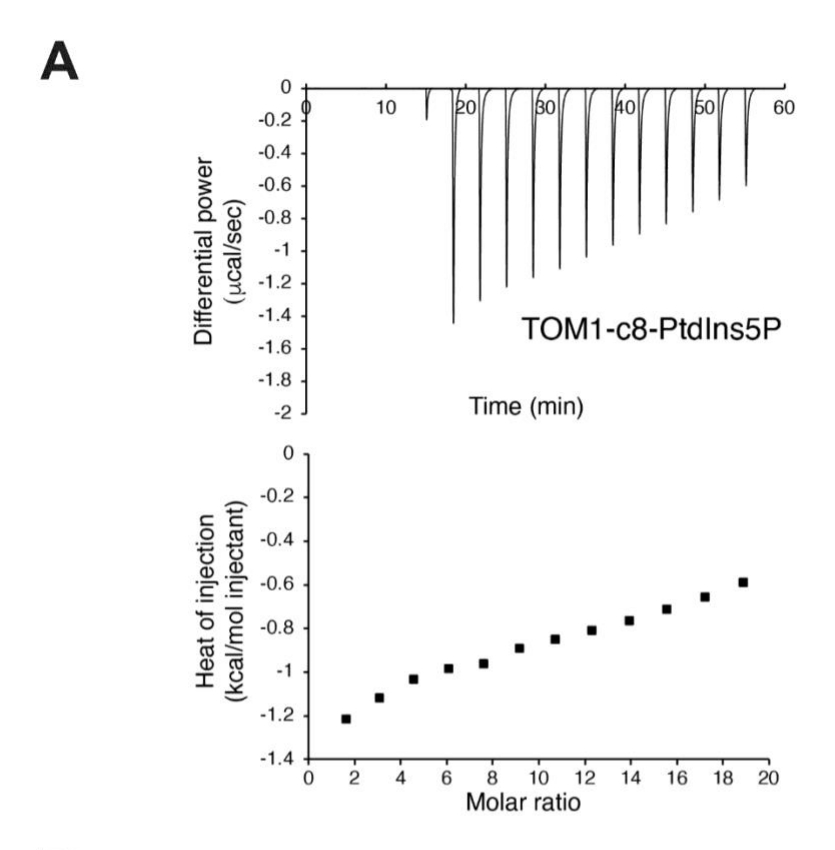


Figure S6. Identification of the ubiquitin-binding site in the TOM1 VHS domain, related to Figure 3. (**A**) Overlay of ¹H-¹⁵N HSQC spectra of the ¹H-¹⁵N TOM1 VHS domain in the absence (red) and presence of 1- (cyan) and 3-fold (black) of ubiquitin. (**B**) A view of the cartoon/surface structure of the TOM1 VHS domain showing residues perturbed by ubiquitin.



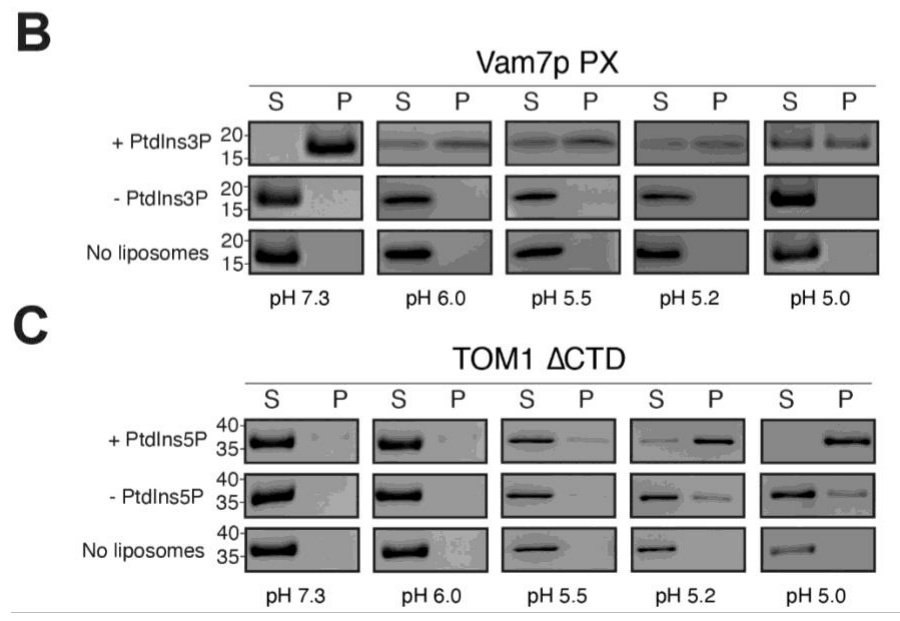


Figure S7. pH-dependent lipid binding properties of TOM1, related to Figures 5 and 6. (A) Calorimetric titration curves for the association of TOM1 to PtdIns5P at pH 7.3. (B) Liposome co-sedimentation assay of the Vam7p PX domain, used as a control, with PtdIns3P-containing (top) or -free (middle) liposomes, or no liposomes (bottom) at the indicated pH values. S, supernatant; P, pellet. (C) Liposome co-sedimentation assay of TOM1 Δ CTD with PtdIns5P-containing (top) or -free (middle) liposomes, or no liposomes (bottom) at the indicated pH values. S, supernatant; P, pellet.

Fig. 6A- PtdIns5P-binding of TOM1 at different pH conditions

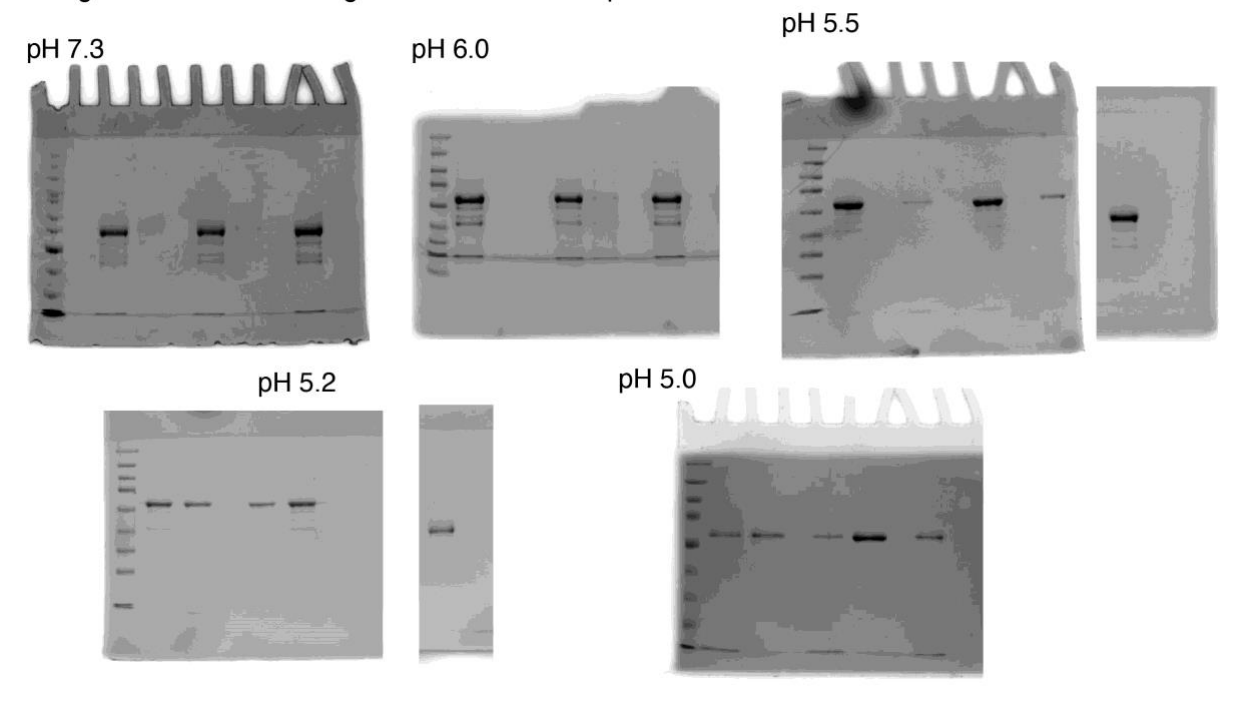


Fig. 6C- PtdIns5P-binding of the TOM1 VHS domain at different pH conditions

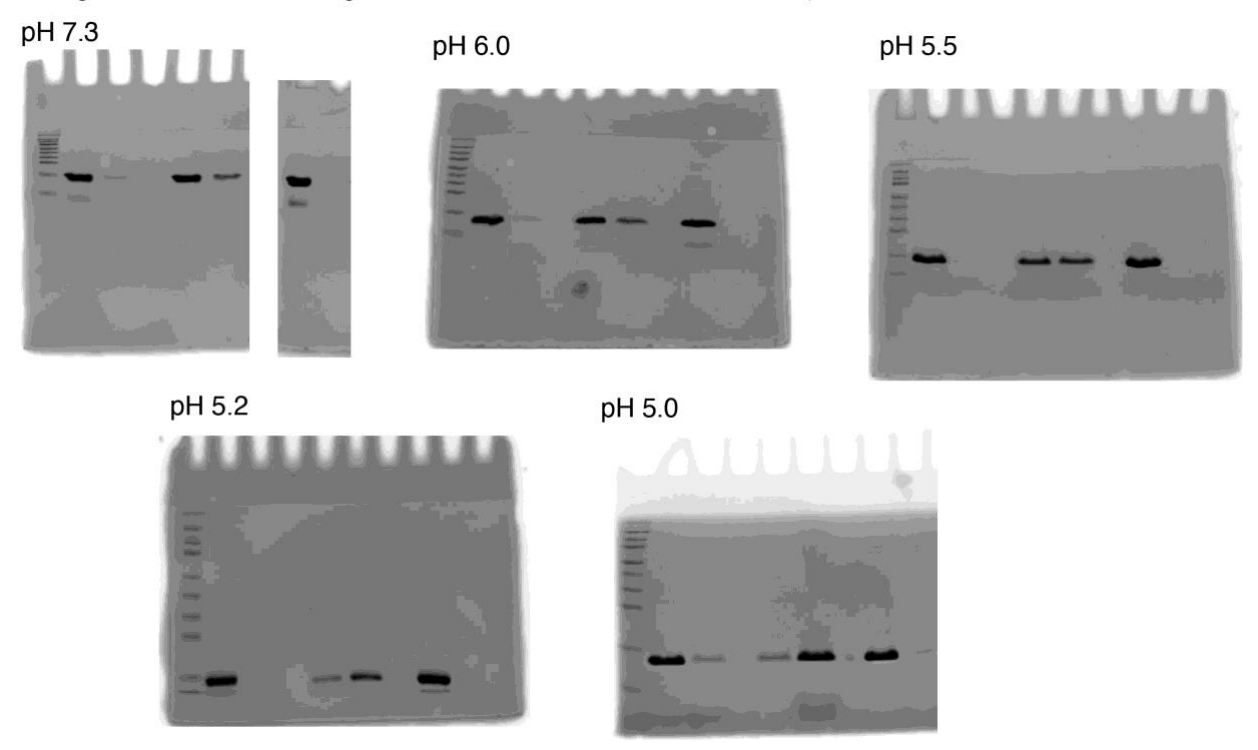


Figure S8. Source data for Figure 6. Full SDS-PAGE gel images corresponding to cropped images shown in Figure 6.

Fig. S7B- PtdIns3P-binding of the Vam7p PX domain at different pH conditions

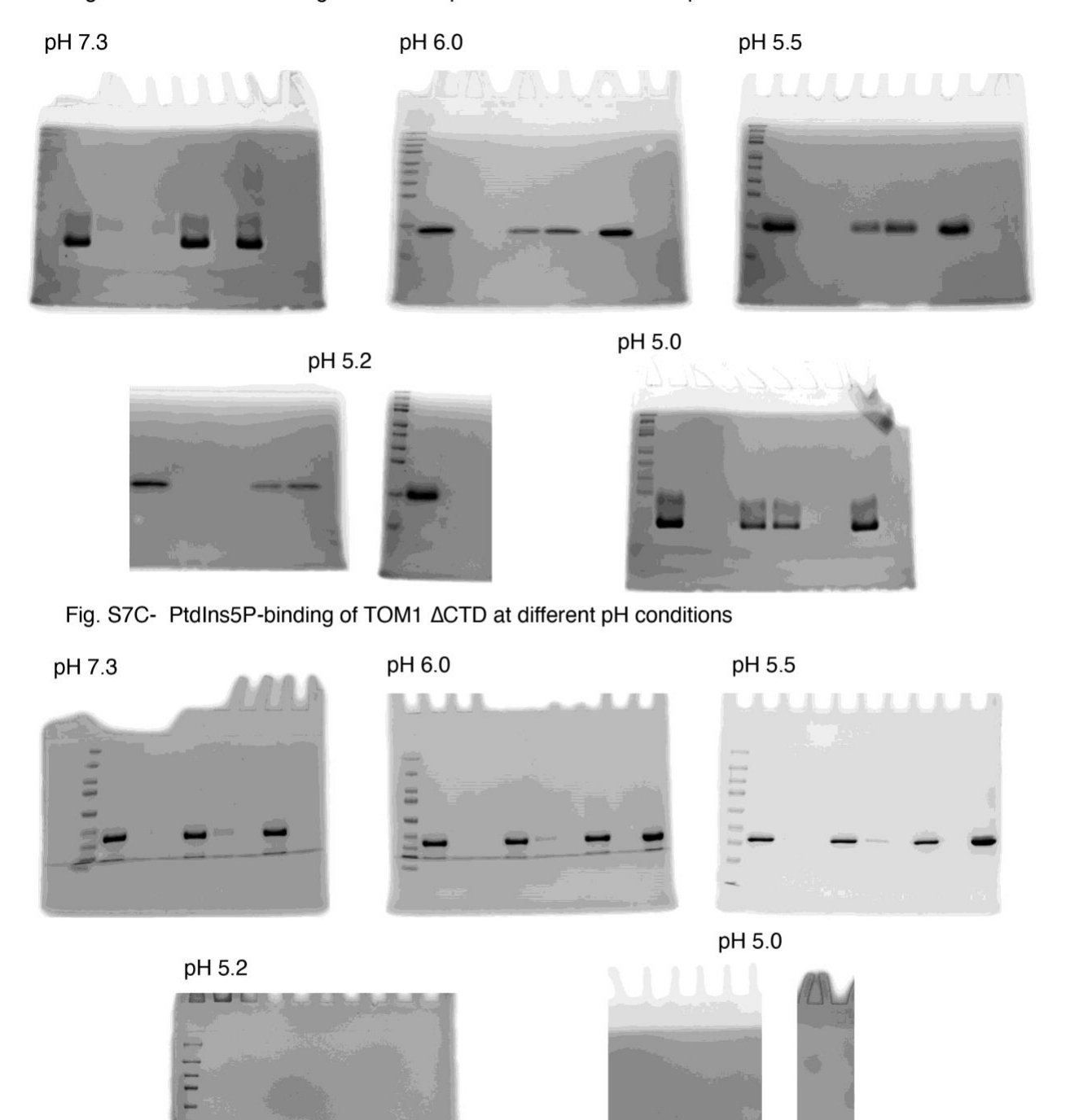
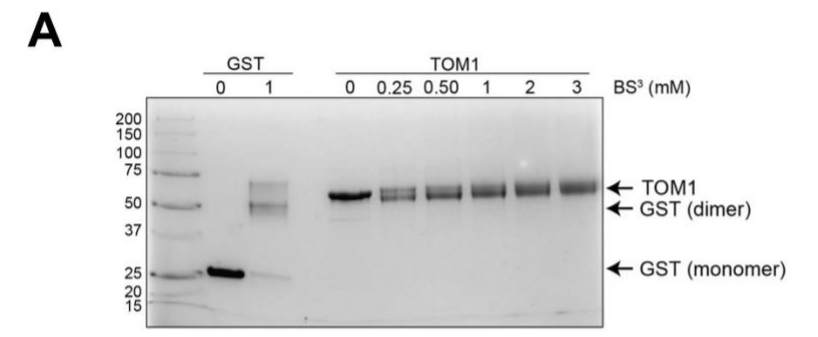
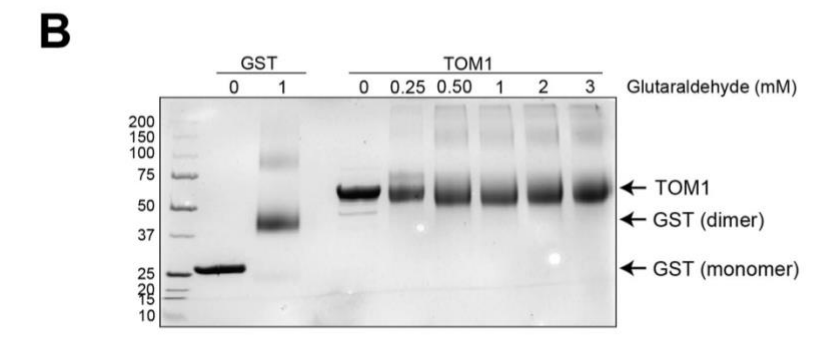


Figure S9. Source data for Figure S7. Full SDS-PAGE gel images corresponding to cropped images shown in Figure S7.





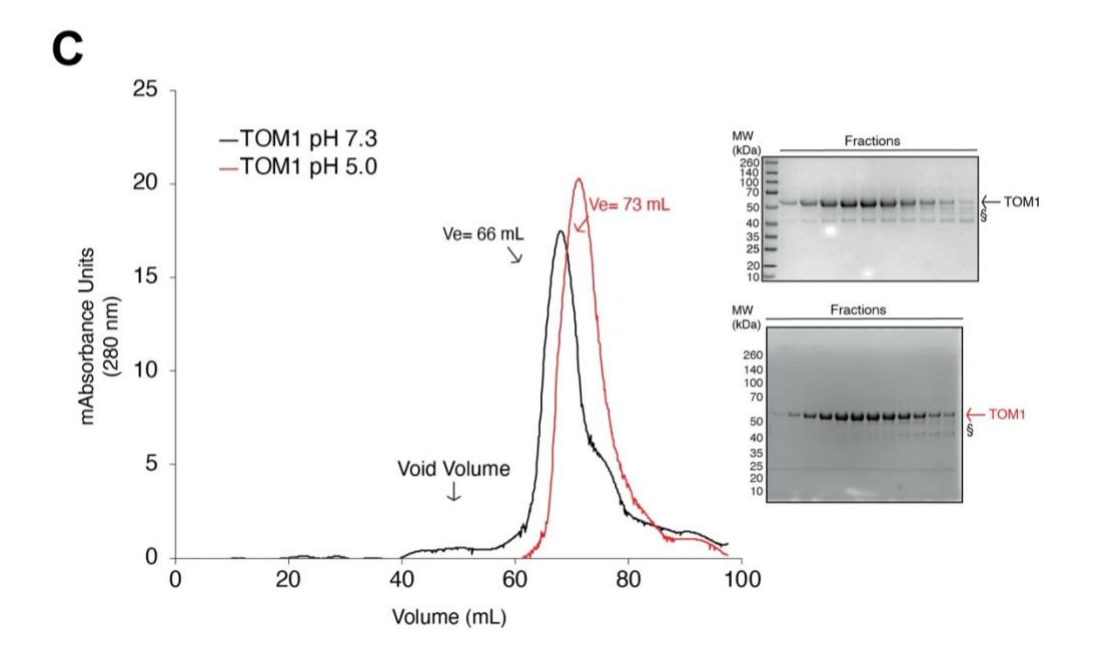
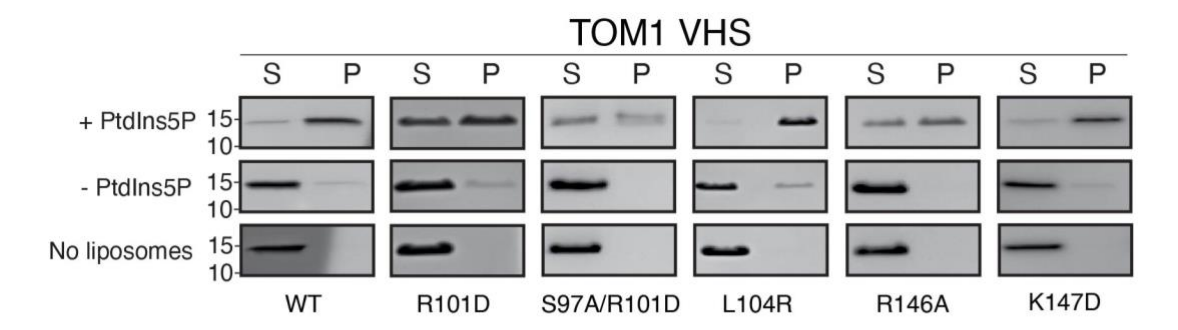


Figure S10. TOM1 does not aggregate nor oligomerize at acidic conditions, related to Figure 6. (A-B) TOM1 was incubated in the absence and presence of the indicated BS³ (A) and glutaraldehyde (B) concentrations at pH 7.3. Oligomer formation was tracked using SDS-PAGE. In both conditions, GST was used as a control. (**C**) Left, size-exclusion chromatogram obtained from a Superdex 200 column, showing the elution profile of TOM1 at pH 7.3 (black) and pH 5.0 (red). The molecular mass of TOM1 could not be estimated due to the CTD-promoted extended shape of the protein. Ve, elution volume. Right, SDS-PAGE analysis of the fractions of each peak at pH 7.3 (top) and pH 5.0 (bottom). § Degradation products.



В

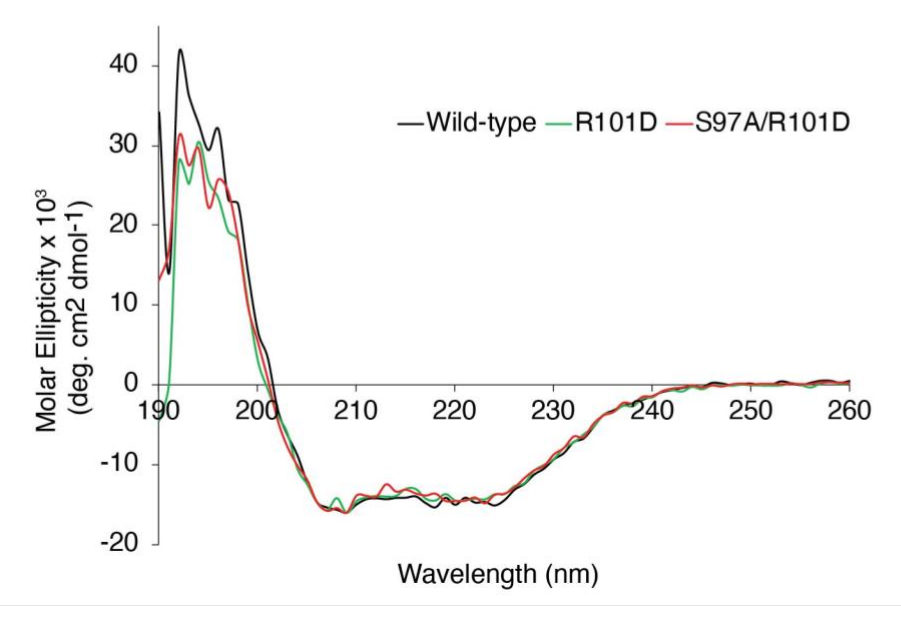


Figure S11. Key PtdIns5P-interacting residues in TOM1 VHS, related to Figures 5 and 6. (A) Liposome co-sedimentation analysis of TOM1 VHS and the indicated mutants using SDS-PAGE. S, supernatant; P, pellet. **(B)** Far-UV CD spectra of TOM1 VHS and the indicated PtdIns5P-binding mutants.

Fig. S11A- Ptdins5P-binding of TOM1 VHS and mutants at pH 5.0

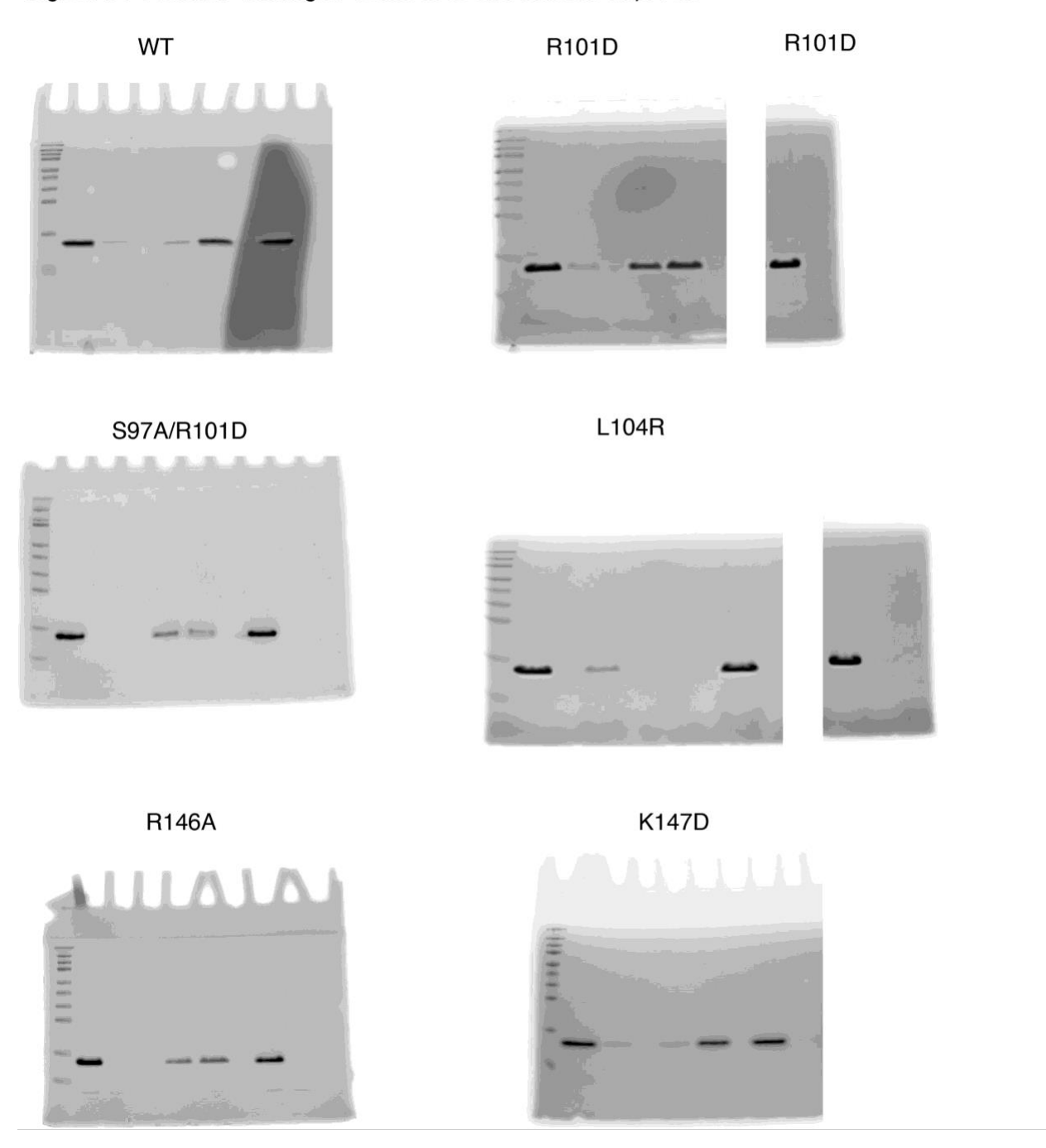


Figure S12. Source data for Figure S11. Full SDS-PAGE gel images corresponding to cropped images shown in Figure S9.

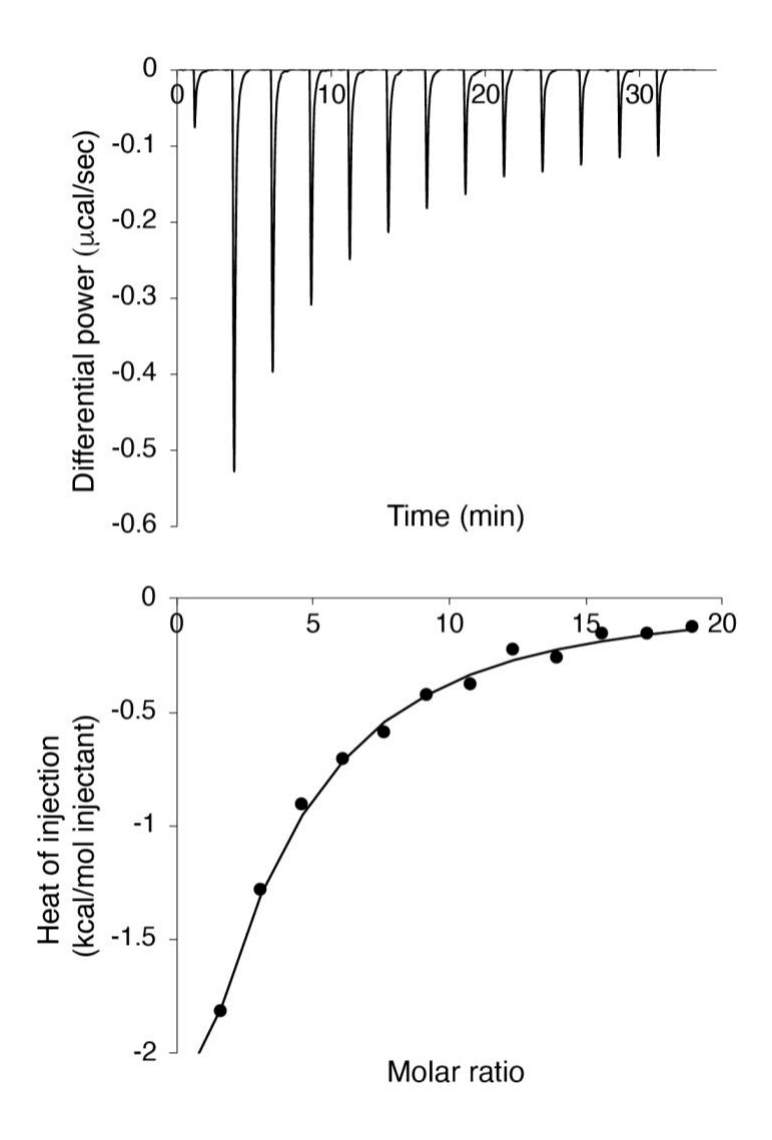


Figure S13. Binding of ubiquitin to TOM1 at pH 7.3 can still be detected at lower TOM1 concentration, related to Figure 7. Calorimetric titration curves for the association of ubiquitin (1 mM) to TOM1 (10 μ M). The upper and lower panels depict the heat change produced upon binding (μ cal/sec), and the integrated binding heat change over the ligand/protein ratio (kcal/mol injectant), respectively. The estimated K_D for this interaction, using the stoichiometry of binding (N) of 2, was $46.0 \pm 5.2 \ \mu$ M.

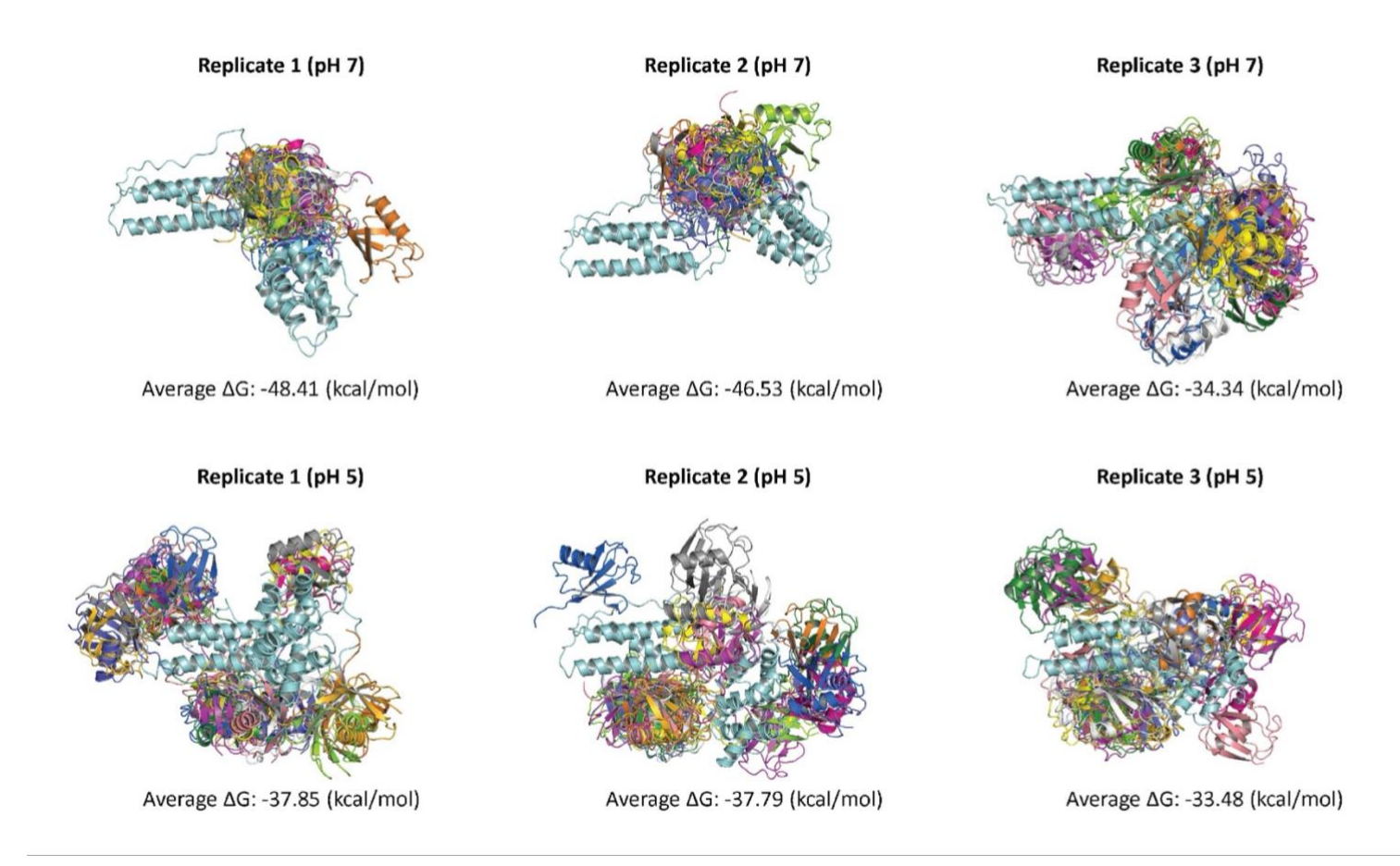
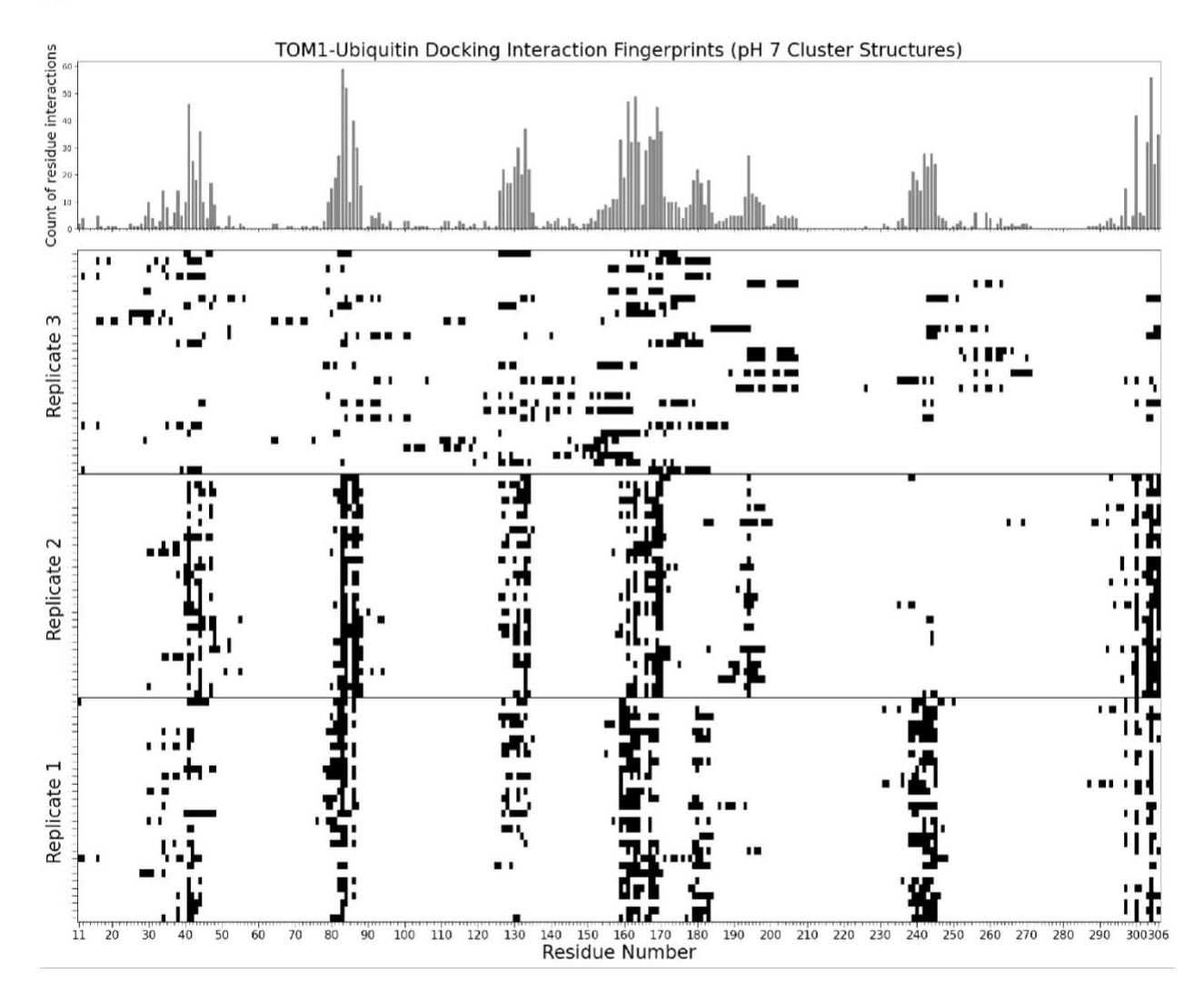


Figure S14. TOM1 (VHS-linker-GAT)-ubiquitin docking poses cluster structures to pH 7 and 5, related to Figure 7. Ubiquitin PDB ID: 1UBQ. The 30 best ubiquitin docking poses are shown on the VHS-linker-GAT region (highlighted in cyan) of the dominant cluster structure for each simulation.







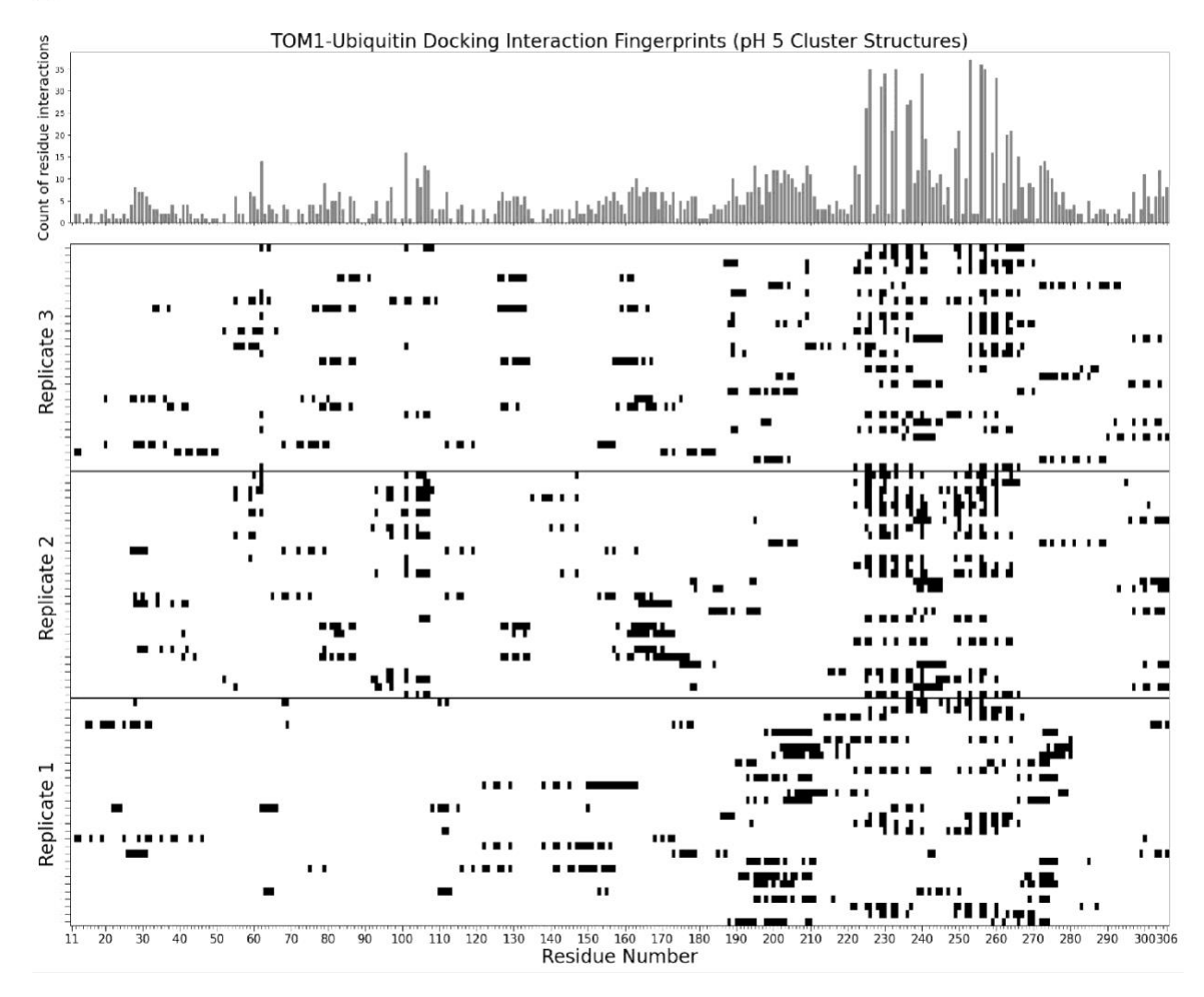
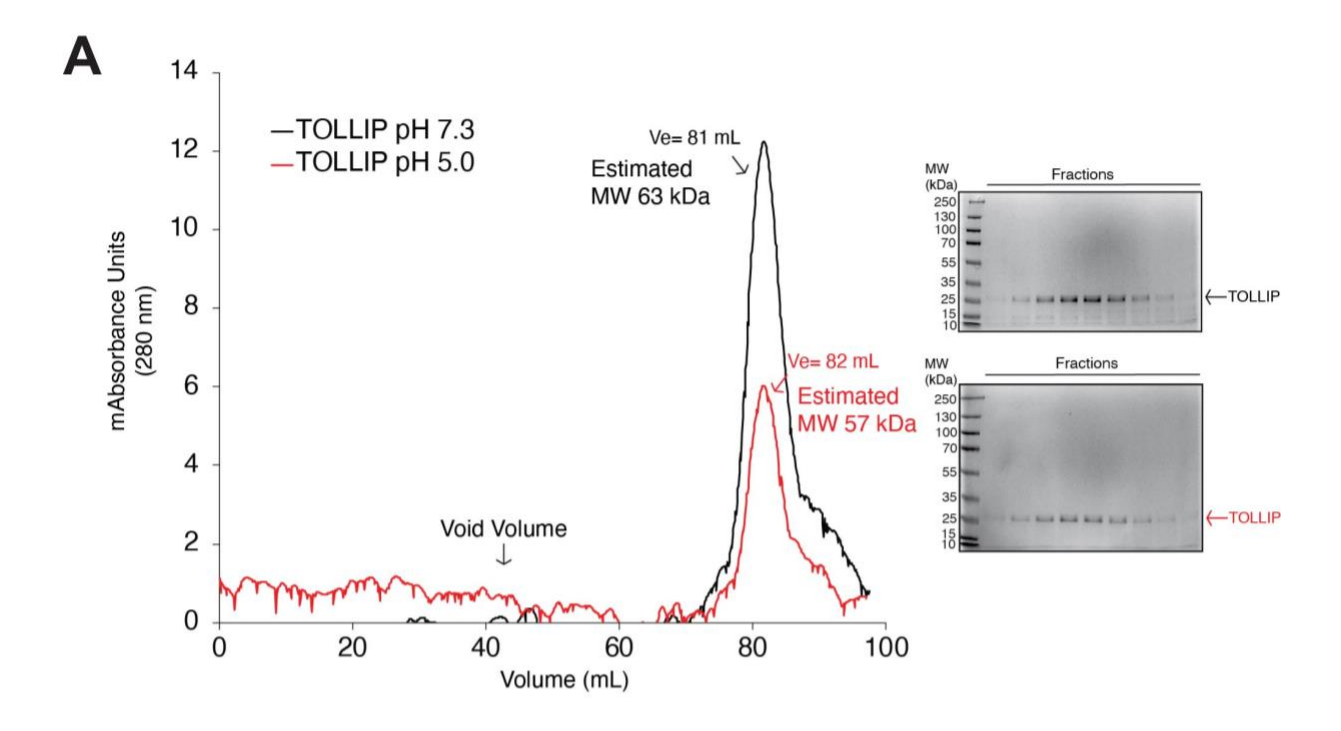


Figure S15. Analysis of the TOM1 interaction with ubiquitin at pH 7 and 5 using docking interaction fingerprints, related to Figure 7. TOM1 (VHS-linker-GAT)-ubiquitin docking interaction fingerprints at pH 7 (**A**) and 5 (**B**). In each case, the interacting residues of TOM1 are shown for the 30 best ubiquitin docking positions to the dominant cluster structure of each replicate. The histogram above displays the number of times each TOM1 residue was involved in ubiquitin docking.



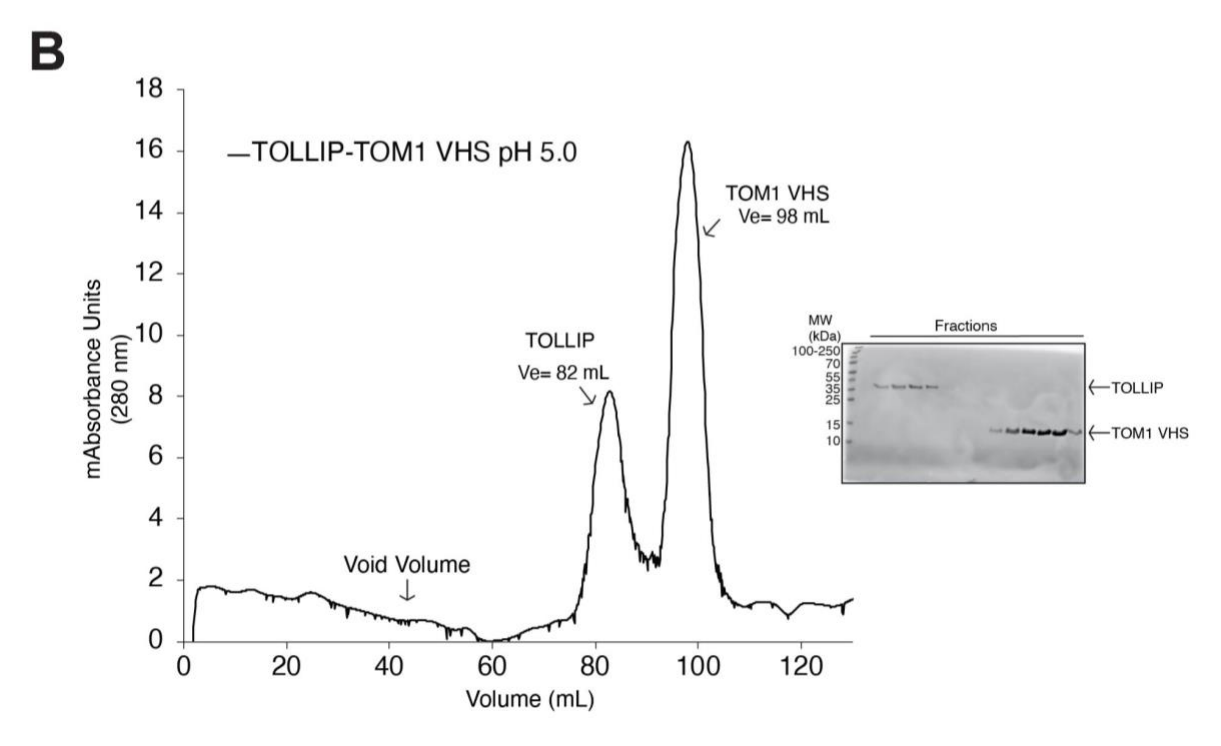


Figure S16. **Features of TOLLIP at acidic conditions, related to Figure 7**. (A) Left, size-exclusion chromatogram obtained from a Superdex 200 column, showing the elution profile of TOLLIP at pH 7.3 (black) and pH 5.0 (red). Ve, elution volume. Right, SDS-PAGE analysis of the fractions of each peak at pH 7.3 (top) and pH 5.0 (bottom). (B) Size-exclusion chromatogram obtained from a Superdex 200 column, showing the elution profile of the TOM1 VHS domain and TOLLIP at pH 5.0. Ve, elution volume. Right, SDS-PAGE analysis of the fractions of each peak.

Fig. 7C- PtdIns5P-binding of TOLLIP at different pH conditions

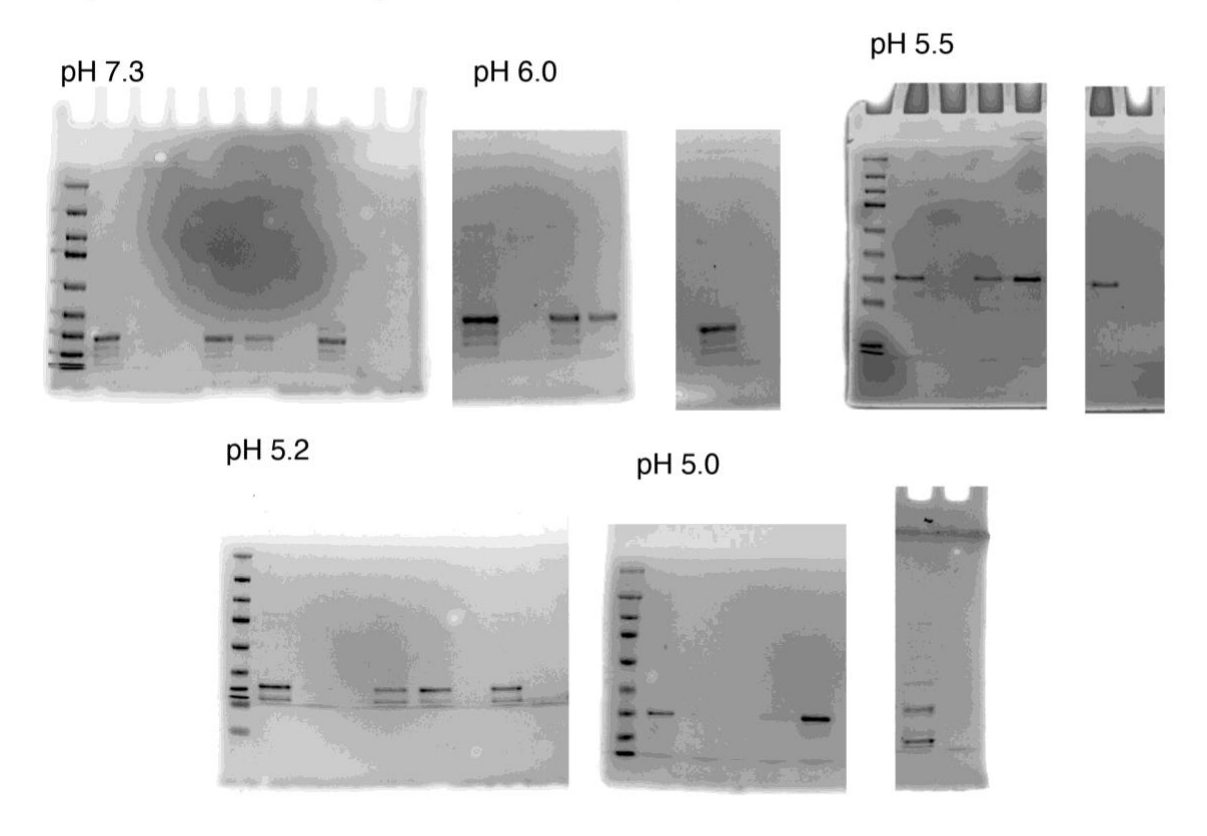


Fig. 7D- PtdIns5P-binding of cross-linked TOM1-TOLLIP at pH 5

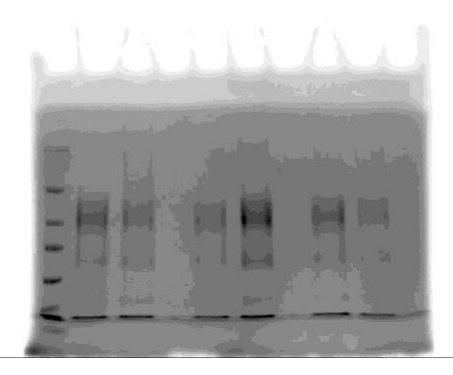


Figure S17. Source data for Figure 7. Full SDS-PAGE gel images corresponding to cropped images shown in Figure 7.

	pH 5 (VHS)	pH 7 (VHS)	pH 5 (GAT)	pH 7 (GAT)	pH 5 (CTD)	pH 7 (CTD)
Replicate 1	1.06	0.98	1.23	0.98	11.48	8.96
Replicate 2	0.96	1.15	1.12	0.76	8.44	10.46
Replicate 3	1.03	1.23	1.29	0.87	13.10	14.61

Table S1. Structural alignment RMSD calculations of TOM1 MD cluster conformations to their initial conformations for each replicate simulation at the indicated pH values, related to Figure 3. Calculations are shown for TOM1 VHS, GAT, and CTD domain alignments.

Interaction	K_{D}	Chi ²
	(M)	
TOM1-TOLLIP	3.3 x 10 ⁻¹⁵	1.0
TOM1 S160D/T164D-TOLLIP	3.4 x 10 ⁻¹⁵	3.3

Table S2. The role of phosphorylation in the TOM1 DXXLL-containing region for TOLLIP binding, related to Figure 4. Kinetic parameters for the binding of TOM1 and TOM1 S160D/T164D to TOLLIP. Values represent the mean of at least two independent experiments.

Primer name	Primer sequence
TOM1 VHS, forward	5' CGCGGATCCTCTCCAGTGGGACAGCGCATCGAGAAAGCC 3'
TOM1 VHS, reverse	5' CCGGAATTCGCCCTACAGGCCTTTCCTCCGCAGGTCCTC 3'
TOM1 GAT, forward	5' GCTCTAGAAAGGAGATATACCATGGAACAGATTGGGAAGCTG 3'
TOM1 GAT, reverse	5' CCATCGATGGTCTGGCCTGTTCGGAACCG 3'
TOM1 VHS-DXXLL, forward	5' CGCGGATCCTCTCCAGTGGGACAGCGCATCGAGAAAGCC 3'
TOM1 VHS-DXXLL, reverse	5' CCGGAATTCCTACACGGTCCTCTGGGGTGTGTGG 3'
TOM1 ΔCTD, forward	5' CGCGGATCCATGGACTTTCTCCTGGGGAACCCGTTC 3'
TOM1 ΔCTD, reverse	5' CCGGAATTCCTAGGTCTGGCCTGTTCGGAACCG 3'
TOM1 linker-GAT, forward	5' CGCGGATCCGAGTTCCCCATGACTGAC 3'
TOM1 linker-GAT, reverse	5' CCGGAATTCCTAGGTCTGGCCTGTTCGGAACCG 3'
TOM1 R101D, forward	5' GAGAGTGTGCTGGTGGACACCATCCTGCCCAAG 3'
TOM1 R101D, reverse	5' CTTGGGCAGGATGGTGTCCACCAGCACACTCTC 3'
TOM1 S97A/R101D, forward	5' GACTTCGTGGAGGCTGTGCTGGTGGACACCATCCTGCCC 3'
TOM1 S97A/R101D, reverse	5' GGGCAGGATGGTGTCCACCAGCACAGCCTCCACGAAGTC 3'
TOM1 L104R, forward	5' GGTGAGGACCATCCGGCCCAAGAACAAC 3'
TOM1 L104R, reverse	5' GTTGTTCTTGGGCCGGATGGTCCTCACC 3'
TOM1 R146A, forward	5' CTATGAGGACCTGCGGGCGAAAGGCCTGTAGGG 3'
TOM1 R146A, reverse	5' CCCTACAGGCCTTTCGCCCGCAGGTCCTCATAG 3'
TOM1 K147D, forward	5' GACCTGCGGAGGGACGGCCTGTAGG 3'
TOM1 K147D, reverse	5' CCTACAGGCCGTCCCTCCGCAGGTC 3'
TOM1 M158A, forward	5' GACTGACCTGGACGCGCTGTCACCCATC 3'
TOM1 M158A, reverse	5' GATGGGTGACAGCGCGTCCAGGTCAGTC 3'
TOM1 M158A/L159A, forward	5' GACCTGGACGCGGCGTCACCCATCCAC 3'
TOM1 M158A/L159A, reverse	5' GTGGATGGGTGACGCCGCGTCCAGGTC 3'
TOM1 D155A/M158A/L159A,	5' GTTCCCCATGACTGCCCTGGACGCGGCG 3'
forward	
TOM1 D155A/M158A/L159A,	5' CGCCGCGTCCAGGGCAGTCATGGGGAAC 3'
reverse	
TOM1 T164D, forward	5' GTCACCCATCCACGATCCCCAGAGGACCG 3'
TOM1 T164D, reverse	5' CGGTCCTCTGGGGATCGTGGATGGGTGAC 3'
TOM1 S160D/T164D, forward	5' GACCTGGACATGCTGGATCCCATCCACGATCCC 3'
TOM1 S160D/T164D, reverse	5' GGGATCGTGGATGGGATCCAGCATGTCCAGGTC 3'
	ı

Table S3. Primers used in this work, related to STAR Methods. Custom primers, which were desalted, were purchased from Thermo Fisher Scientific.